



RESEARCH ARTICLE

10.1029/2023MS003738

Special Section:

Using radiative-convective equilibrium to understand convective organization, clouds, and tropical climate

Key Points:

- A satellite simulator is successfully modified for use with offline model output of atmospheric profiles
- The high-cloud altitude feedback is positive and is the main contributor to the total cloud feedback in radiative-convective equilibrium (RCF)
- Tropical cloud feedbacks are well-captured by RCE

Supporting Information:

Supporting Information may be found in the online version of this article.

Correspondence to:

C. L. Stauffer, cls14b@fsu.edu

Citation:

Stauffer, C. L., & Wing, A. A. (2023). Explicitly resolved cloud feedbacks in the Radiative-Convective Equilibrium Model Intercomparison Project. *Journal of Advances in Modeling Earth Systems*, 15, e2023MS003738. https://doi.org/10.1029/2023MS003738

Received 29 MAR 2023 Accepted 16 OCT 2023

Author Contributions:

A. Wing
Data curation: A. A. Wing
Formal analysis: C. L. Stauffer
Investigation: C. L. Stauffer
Methodology: C. L. Stauffer, A. A. Wing
Resources: A. A. Wing

Conceptualization: C. L. Stauffer, A.

© 2023 The Authors. Journal of Advances in Modeling Earth Systems published by Wiley Periodicals LLC on behalf of American Geophysical Union. This is an open access article under the terms of the Creative Commons Attribution License, which permits use, distribution and reproduction in any medium, provided the original work is properly cited.

Explicitly Resolved Cloud Feedbacks in the Radiative- Convective Equilibrium Model Intercomparison Project

C. L. Stauffer¹ and A. A. Wing¹

¹Department of Earth, Ocean and Atmospheric Science, Florida State University, Tallahassee, FL, USA

Abstract Radiative-convective equilibrium (RCE) is particularly well suited for studying tropical deep-convection, a regime of clouds that contributes some of the highest uncertainties to the estimates of total cloud feedback. In order to perform a comprehensive calculation and decomposition of cloud feedbacks in cloud-permitting models, previously primarily done in global climate models, the configuration of a satellite simulator for use with offline data was successfully implemented. The resultant total cloud feedback is slightly positive, primarily driven by the longwave effects of increases in cloud altitude. The high-cloud altitude feedback is robustly positive and has a central value and uncertainty well-matched with prior estimates. Reductions in high cloud amount drive a tropical anvil cloud area feedback that is on average negative, consistent with prior estimates. However, a subset of models with finer horizontal grid spacing indicate that a positive tropical anvil cloud area feedback cannot be ruled out. Even though RCE is only applicable to tropical deep-convective clouds, the RCE total cloud feedback is within the range of prior comprehensive estimates of the global total cloud feedback. This emphasizes that the tropics heavily influence the behavior of global cloud feedbacks and that RCE can be exploited to learn more about how processes related to deep convection control cloud feedbacks.

Plain Language Summary Clouds act to simultaneously cool and warm the environment by blocking sunlight from reaching the surface as well as preventing the Earth from emitting heat away from the surface. When the surface temperature warms, different properties of the clouds change in different ways, causing their warming and cooling effects to change. How strongly the clouds cool or warm the surface in a warming climate is the number one source of uncertainty in estimates of the total change in surface temperature to a forced change. This is primarily due to the difficulty the models that are typically used have in simulating clouds. Here, a special kind of model that more accurately simulates clouds is used to study the impact of cloud changes on the total surface warming. Clouds act to warm the environment primarily due to the upward shift in height clouds undergo in a warmer environment.

1. Introduction

Uncertainty in cloud feedbacks, especially those associated with tropical and maritime convection (Vial et al., 2013), estimated by global climate models (GCMs) has consistently been identified as the largest source of uncertainty in climate sensitivity (Dufresne & Bony, 2008; Sherwood et al., 2014; Soden & Held, 2006; Soden & Vecchi, 2011; Zelinka et al., 2013). This is mainly attributed to the necessity for GCMs to implement cloud and convection parameterization schemes due to their coarse horizontal resolution, which is not able to resolve the scales of cloud processes (Li et al., 2012; Waliser et al., 2009). Despite improvements in models being implemented in the release of phase six of the Coupled Model Intercomparison Project (CMIP6; Eyring et al., 2016), the spread in climate sensitivity across those models has only increased, which has been attributed to the role of clouds; in particular, increases in uncertainty in the low-cloud feedback (Sherwood et al., 2020; Zelinka et al., 2020). A recent expert assessment of climate sensitivity and feedbacks used a Bayesian approach to combine multiple lines of evidence, including observations, paleoclimate records, GCM simulations, and high-resolution process modeling (Sherwood et al., 2020). This expert assessment identified feedbacks associated with tropical deep convection (e.g., anvil clouds) as the largest source of uncertainty in climate feedback estimates as a whole. While understanding of processes contributing to cloud feedbacks has advanced (e.g., Dessler, 2013; Myers et al., 2021; Tsushima et al., 2014; Zelinka et al., 2020), the persistent uncertainty highlights the continued need to improve understanding of convective processes and their representation in climate models, especially those governing changes in tropical deep-convective clouds (Bony et al., 2015). In this study we examine the cloud feedbacks that occur in high resolution models configured to explicitly model tropical convection.

STAUFFER AND WING 1 of 24



10.1029/2023MS003738

Software: C. L. Stauffer
Supervision: A. A. Wing
Validation: C. L. Stauffer, A. A. Wing
Visualization: C. L. Stauffer
Writing – original draft: C. L. Stauffer
Writing – review & editing: C. L.
Stauffer, A. A. Wing

Longwave radiation emitted by cloud tops is proportional to cloud top temperature. When the surface warms, cloud tops are expected to rise approximately isothermally following the Fixed Anvil Temperature, or FAT, hypothesis (Hartmann & Larson, 2002). This is because anvil clouds are found where the radiative cooling rate rapidly decreases with height, which is constrained by the water vapor profile and thus linked to temperature via the Clausius-Clapeyron relationship. However, the increase in static stability of the upper atmosphere in a warmer climate modifies this to cause cloud tops to warm slightly, at a slower rate than the surface (the Proportionally Higher Anvil Temperature, or PHAT, hypothesis; Zelinka & Hartmann, 2010). This would cause a positive top of atmosphere radiative anomaly due to the reduction of outgoing longwave radiation (OLR) associated with the cooler cloud tops compared to if the cloud tops warmed in step with the surface. While some assumptions underlying FAT/PHAT have been questioned recently (Jeevanjee & Zhou, 2022; Seeley, Jeevanjee, Langhans, & Romps, 2019; Seeley, Jeevanjee, & Romps, 2019), the expectation that cloud tops rise and warm less than the surface remains (e.g., Aerenson et al., 2022; Kuang & Hartmann, 2007; Stauffer & Wing, 2022; Wetherald & Manabe, 1988; Zelinka & Hartmann, 2011).

Changes in cloud amount with warming are less certain. One theory, based in similar principles as PHAT and entitled the "stability iris" theory, suggests that anvil spreading is mechanistically controlled by the vertical gradient of clear-sky subsidence (Bony et al., 2016). In the clear-sky region of the tropics, warming by large-scale subsidence is required to offset radiative cooling. By mass continuity, the vertical divergence of this clear-sky subsidence is provided by the divergence of the upward deep-convective mass flux, and therefore anvil spreading. In a warming environment, increases in static stability mean that less subsidence is required to balance the radiative cooling, and thus less convective outflow occurs. Decreases in cloud amount would enhance OLR and increase the amount of solar radiation reaching the surface causing both cooling and warming in the longwave and shortwave, respectively. Some observational studies have identified a decrease in anvil coverage with warming (e.g., Igel et al., 2014; Zelinka & Hartmann, 2011), consistent with this theory.

Many of the numerical studies that have investigated these cloud property changes have utilized an idealized framework of the tropical atmosphere called radiative-convective equilibrium (RCE). RCE is a statistical balance between radiative cooling and convective heating ideally suited to study tropical deep convection (Jakob et al., 2019; Tompkins & Craig, 1998). One limitation of RCE simulations is that they typically do not capture all regimes of clouds, such as stratocumulus, which is a regime that has been identified as one of the most important contributors to the uncertainty in the cloud feedback (in particular, the low-cloud feedback; Bony & Dufresne, 2005; Qu et al., 2014; Webb et al., 2006). Thus, RCE is best suited to aiding expert assessment of the cloud feedbacks associated with tropical deep-convecting clouds, such as the high-cloud altitude and cloud amount feedbacks that remain highly uncertain (Sherwood et al., 2020; Zelinka et al., 2020, 2022). By eliminating complications from heterogeneous boundary conditions or forcing and the resulting large-scale dynamical instabilities, the idealization of RCE is an essential component in model hierarchies (Jeevanjee et al., 2017; Maher & Gerber, 2019), in which understanding is built in simpler settings that can be connected across systems of incrementally increasing complexity (Held, 2005).

The simplifications of the climate system permitted within RCE simulations supports a range of horizontal resolutions from GCM-scale to less than 1 km (Becker & Wing, 2020; Cronin & Wing, 2017; Tompkins & Craig, 1998; Wing et al., 2020a). The Radiative-Convective Equilibrium Model Intercomparison Project (RCEMIP; Wing et al., 2018, 2020a) is an unprecedented collection of several types of models, including those that parameterize convection as well as those that explicitly resolve convection, all commonly configured in this framework. In all the models examined in RCEMIP, the anvil clouds (defined as the upper troposphere maximum in cloud fraction) increased in altitude, either isothermally or with slightly higher temperature (Stauffer & Wing, 2022). Approximately two-thirds of the models displayed a decrease in cloud fraction with warming sea surface temperature (SST) and were shown to mostly follow the stability iris theory presented above.

With foundational understanding of how clouds are expected to change with warming SST presented consistently across RCE simulations, the natural next step is to quantify the cloud feedbacks that result from these changes. Previous RCE studies have generally been limited to approximating cloud feedbacks by describing changes in the cloud radiative effect (Becker & Wing, 2020), or by analyzing the processes that cause high clouds to change with warming (Ohno et al., 2019, 2020, 2021; Ohno & Satoh, 2018). Becker and Wing (2020) used RCEMIP to focus on the causes of spread in climate sensitivity in those models. They used the cloud radiative effect and climate feedback parameter and found that changes in shallow cloud fraction, and its effect on shortwave fluxes,

STAUFFER AND WING 2 of 24

explained a large portion of the climate sensitivity spread in RCEMIP CRMs. However, simply examining the change in the cloud radiative effect cannot provide the complete picture of cloud impacts on climate (Cess & Potter, 1988) and relatively few studies have performed a comprehensive calculation of cloud feedbacks in models with explicit convection. One such study, Cronin and Wing (2017), used temperature and water vapor kernels to compute a kernel-corrected cloud feedback (Soden et al., 2004) for a cloud resolving model (CRM) configured in RCE (which, to the best of our knowledge, is the only study that has used a CRM in RCE to explicitly calculate cloud feedbacks), and found that the kernel correction was important for making the total cloud feedback positive.

A few other studies using different model configurations (non-RCE) that explicitly simulated convection have also quantified cloud feedbacks. In one such series, using the global model NICAM with explicit convection at 7 and 14 km horizontal grid spacing, the longwave cloud feedback for clouds with a cloud-top pressure (CTP) less than 440 hPa was found to be 1.7 W m⁻² K⁻¹ (Tsushima et al., 2014) which is stronger than that found in CMIP3 (-0.1 to 0.9 W m⁻² K⁻¹; Zelinka et al., 2012a). This is primarily associated with an *increase* in high clouds (as opposed to the decrease found in GCMs), regardless of the baseline amount of high clouds (NICAM tends to overestimate while the GCMs underestimate). In a different set of NICAM experiments, Chen et al. (2016) instead found the longwave cloud feedbacks for clouds with CTP less than 440 hPa to be \sim 0.60 W m⁻² K⁻¹, which lies within the uncertainty of the average of CMIP5/CFMIP2 (the second phase of the Cloud Feedback Model Intercomparison Project). They found that the cloud feedback tends to be sensitive to the horizontal grid spacing (also found in Noda et al., 2014; Zhou et al., 2014), the microphysics scheme implemented, and the treatment of the ice radii (whether it is fixed or a profile). This is also consistent with results found in Jeevanjee and Zhou (2022).

In addition to sensitivity to microphysics schemes, a comprehensive decomposition of the cloud feedback was found to be sensitive to boundary layer and turbulence schemes within a super-parameterized (SP) model (Bretherton & Blossey, 2014). For this model, unlike in NICAM, the longwave (and shortwave) cloud feedback were moderately positive (0.30 and 0.19 W m⁻² K⁻¹, respectively) and comparable to the traditional GCM version of the SP model as well as the model mean cloud feedbacks in CMIP5 (Zelinka et al., 2013). Here, the impact on the longwave by increases in high cloud altitude explains a large portion (relative to other components of the feedback) of the total net cloud feedback. (Note, the values for Tsushima et al. (2014) are limited to the tropics while the values for Bretherton and Blossey (2014) are a global average.)

Despite the limited applicability of RCE, there is merit to using RCE as a simplified framework of the tropical climate that is ideally situated to study deep-convection and its impact on the cloud feedbacks. RCEMIP is an unprecedented collection of commonly-configured models run in RCE which presents the opportunity to elucidate further understanding of the cloud feedbacks associated with tropical deep-convecting clouds. In particular, the inclusion of models with explicit convection in RCEMIP may add another source of information to assessments and conclusions about the cloud feedback. This study seeks to understand cloud feedbacks in RCE by performing an explicit calculation of cloud feedbacks across RCEMIP simulations. This, to the best of our knowledge, is the first time such a calculation has been performed across an ensemble of CRMs. Section 2 describes the RCEMIP data set while Sections 3 and 4 describe the implementation of an offline satellite simulator and cloud radiative kernels suitable for this type of model simulation. Sections 5 and 6 characterizes the cloud feedbacks and their decomposition in RCE and compares them to those derived by CMIP models before closing with a discussion in Sections 7 and 8.

2. The RCEMIP Archive

The RCEMIP archive (Wing et al., 2018, 2020a) consists of over 30 models consistently configured in the RCE framework. There are models with explicit convection as well as models with parameterized convection, however, the nature of the cloud feedback computation (described in Sections 3 and 4) limits the models used to the models with explicit convection that provide instantaneous 3D snapshots. Specifically, the data fields used are six-hourly instantaneous 3D snapshots of temperature, pressure, water vapor (specific humidity), cloud liquid water, and cloud ice water from the last \sim 25 days of the simulations, where the metrics used in this study are temporally averaged from this range. The resolution of the GCMs (\sim 1° × 1°) is too coarse to resolve clouds, requiring the implementation of a parameterization. This requires an assumption of the sub-grid scale distribution of clouds which does not have an offline capability and the grid box-averaged cloud water content is not suitable for use in offline radiation calculations, as required for the cloud feedbacks calculated in this study.

STAUFFER AND WING 3 of 24

For the models with explicit convection, there is a "small" domain (RCE_small, $\sim 100 \times 100 \text{ km}^2$ with 1 km horizontal resolution and ~ 74 vertical levels), in which aggregation isn't expected to spontaneously organize (self-aggregation), and a "large" domain (RCE_large, $\sim 6,000 \times 400 \text{ km}^2$ with 3 km horizontal resolution and ~ 74 vertical levels), where convection does aggregate, that is initialized from a profile that is temporally- and domain-averaged from the RCE_small simulations. Each simulation is run at three different SSTs (295, 300, and 305 K) to represent different climates. The SST is constant everywhere and remains uncoupled with the atmosphere. The focus of this study is to establish fundamental expectations for cloud feedbacks in RCE without considering the influence of organized convection and so will focus on the 12 CRM RCE_small simulations, four small domain CRMs with a higher vertical resolution (RCE_small_vert, ~ 146 levels), and three small domain large eddy simulations (LES) with a higher vertical and horizontal resolution (RCE_small_les, 200 m horizontal resolution and ~ 146 levels). The convection in all the simulations examined here remains unorganized. More details on the RCEMIP simulations can be found in the protocol and overview papers (Wing et al., 2018, 2020a).

3. The ISCCP Histogram

The cloud feedbacks are calculated following the procedures of Zelinka et al. (2013), which uses histograms from the International Satellite Cloud Climatology Project simulator (ISCCP; Klein & Jakob, 1999; Webb et al., 2001) and cloud radiative kernels partitioned into 49 CTP and optical depth (τ) bins. Cloud radiative kernels relate perturbations in cloud amount of each type to the associated radiative effect. The RCEMIP protocol did not call for any satellite simulator to be run, nor do all the models necessarily have the means to implement satellite simulators in general, necessitating the need to create a simulator for use with offline data, described below and in Appendix A. It is useable with any data set that has profiles of temperature, cloud water, and water vapor.

3.1. The Offline ISCCP Simulator

As detailed in Appendix A, the procedure for calculating cloud optical depth and CTP offline are identical to the current online implementation of the ISCCP simulator (Klein & Jakob, 1999; Webb et al., 2001), except the algorithm is simplified by excluding the clear-sky brightness temperature procedures which were later added to the simulator following Schwarzkopf and Ramaswamy (1999). Also, rather than using the look-up tables for the shortwave cloud optical depth and longwave emissivity parameterizations (as used by SAM-CRM's interface with the online ISCCP simulator), the offline simulator uses the equations directly from Fu (1996) and Slingo (1989), which are the same parameterizations, just implemented differently. The decision to exclude the clear-sky brightness temperature procedures was to create a simulator as simple as possible using easily-understood radiative transfer concepts (i.e., return to the original design and implementation of Klein & Jakob, 1999).

In addition to the models from the RCEMIP archive, new simulations of SAM6.11.2 (Khairoutdinov & Randall, 2003), following the RCEMIP protocol (Wing et al., 2018), are used. These auxiliary simulations, referred to as SAM-CRM-COSP, implement the ISCCP simulator (Klein & Jakob, 1999; Webb et al., 2001) online, which is used to test the development of an Approximate ISCCP Simulator (AIS, described below) for use with offline data.

Figure 1 compares spatial maps of brightness temperature (used to find CTP, Figures 1a-1c) and CTP (Figures 1e-1g) using the offline process including (Offline ISCCP Simulator, "OIS," Figures 1a and 1e) and excluding (Approximate ISCCP Simulator, "AIS," Figures 1b and 1f) the clear-sky brightness temperature procedures, as well as the difference between the two methods (Figures 1c and 1g). This difference is small (relative to the values of brightness temperature and CTP) and is primarily concentrated outside of areas with wide-spread clouds (e.g., the convection centered around the red cross in Figures 1a-1c and 1e-1g has a difference of zero almost everywhere). Visually, all the features appear in both versions of the simulator (such as the previously identified convection) and, although there are areas where the magnitudes differ, the regions of deepest convection are near-identical and the largest differences tend to occur on the outer parts of the convective regions where CTP and T_p are highest. The point-wise correlation between the two methods is displayed by plotting the values of T_R or CTP of AIS versus OIS in Figures 1d and 1h. Each gray circle is a grid point, the black dotted line is the one-to-one line, and the blue solid line is the line of best fit. The two simulators are highly correlated, and the primary deviation occurs for the warmest T_R values, associated with a stronger deviation in the higher CTP values. This deviation is also seen in the PDFs of the variables (Figure 2). Although AIS has smaller maxima in its brightness temperature distributions, the largest difference is only transposed onto the higher CTP (lower clouds) for the CTP distribution (and, primarily in the highest CTP bin, given by the right-most vertical dashed

STAUFFER AND WING 4 of 24

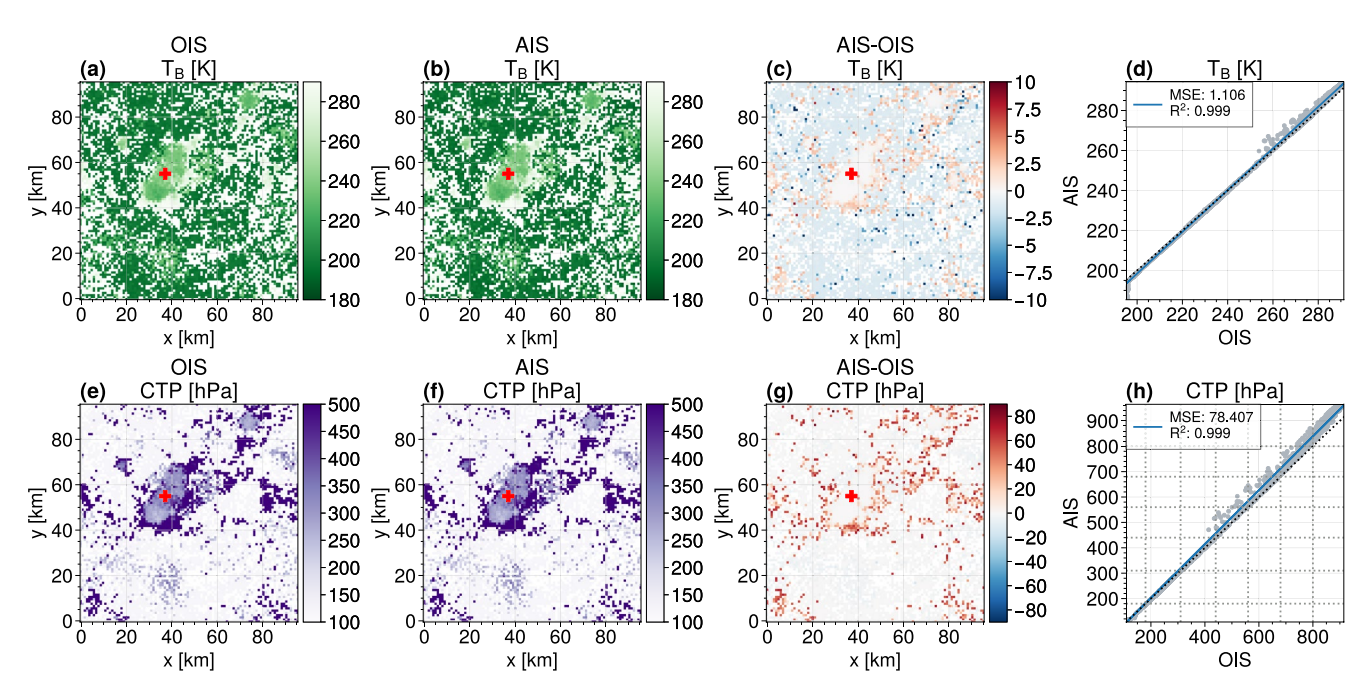


Figure 1. Snapshots of brightness temperature (T_B) (a–c) and cloud-top pressure (CTP) (e–g) for the Offline ISCCP Simulator (OIS) (a, e) and Approximate ISCCP Simulator (AIS) (b, f), which excludes clear-sky brightness temperature processes, and the difference between the two versions (c, g). The red cross in panels (a–c, e–g) identifies a common feature between the two methods referred to in the text. The spatial correlation between AIS and OIS for T_B (d) and CTP (h) is given by the coefficient of determination of the line of best fit between the two simulators (blue solid line). The dotted black line in panels (d, h) is the one-to-one line. The data is from day 3.75 of a RCE_small 300 K simulation of SAM-CRM-COSP where the 2D output was saved at the same frequency as the 3D output.

gray line in Figure 2b). Even as AIS shifts the distribution toward higher pressures, the high cloud distribution, the region most relevant in RCE, is remarkably consistent between AIS and OIS, as seen in the correlations between the two methods (Figures 1d and 1h).

The difference between the offline version and the online version of the ISCCP simulator can be analyzed by looking at its impact on the ISCCP histograms of AIS, OIS, and SAM-CRM-COSP (where the ISCCP simulator was run online). OIS differs from the online implementation in that OIS is limited to the six-hourly instantaneous output while COSP is run online, with the radiation scheme, at a temporal frequency of minutes; that is, the temporal sampling of the data is coarser in OIS (and AIS). Stauffer and Wing (2022) used the six-hourly snapshots to recompute cloud fraction for the RCEMIP CRMs. They found that, although a slight bias is introduced when using the limited temporal sampling, the differences are small and the conclusions from use of the profiles in their analysis remained unchanged. Additionally, all calculations made are used across the models, which may differ from what an individual model's native implementation may be.

Figures 3a–3c and 3e–3f compares the ISCCP histograms of SAM-CRM-COSP to OIS and SAM-CRM-COSP to AIS and Figures 3b–3d compares the ISCCP histograms of OIS to AIS. The offline versions shift the high-thin clouds upwards (the dipole of decreases and increases in cloud amount in the optically thinnest bin), but otherwise does a decent job capturing the relative distribution of cloud amount in CTP-τ space. AIS also holds up almost perfectly to OIS (Figures 3d–3f) and the difference in the cloud feedbacks are minimal (not shown), justifying the use of the simplified version of the simulator (AIS), which is the version applied to the remaining models and discussed in the remainder of this study.

3.2. The ISCCP Histogram Distribution

Although there are vast differences in the ISCCP histogram from model to model (Figure 4 shows the histograms for each model for the 300 K simulations and Figures S1 and S2 in Supporting Information S1 shows the histograms for the 295 and 305 K simulations, respectively), there is one clear characteristic common across the models: the cloud distribution is dominated by high and thin to medium-thick clouds. These clouds are probably anvil or detached anvils formed by deep convection and have been classified in the earliest use of ISCCP as cirrus-type clouds (Hahn et al., 2001; Rossow & Schiffer, 1991). Specifically, the highest (or one of the highest) concentrations

STAUFFER AND WING 5 of 24

19422466, 2023, 11, Downloaded from https://agupubs.onlinelibrary.wiley.com/doi/10.1029/2023MS003738, Wiley Online Library on [05/12/2023]. See the Terms and Conditions (https://onlinelibrary.wiley.com/terms

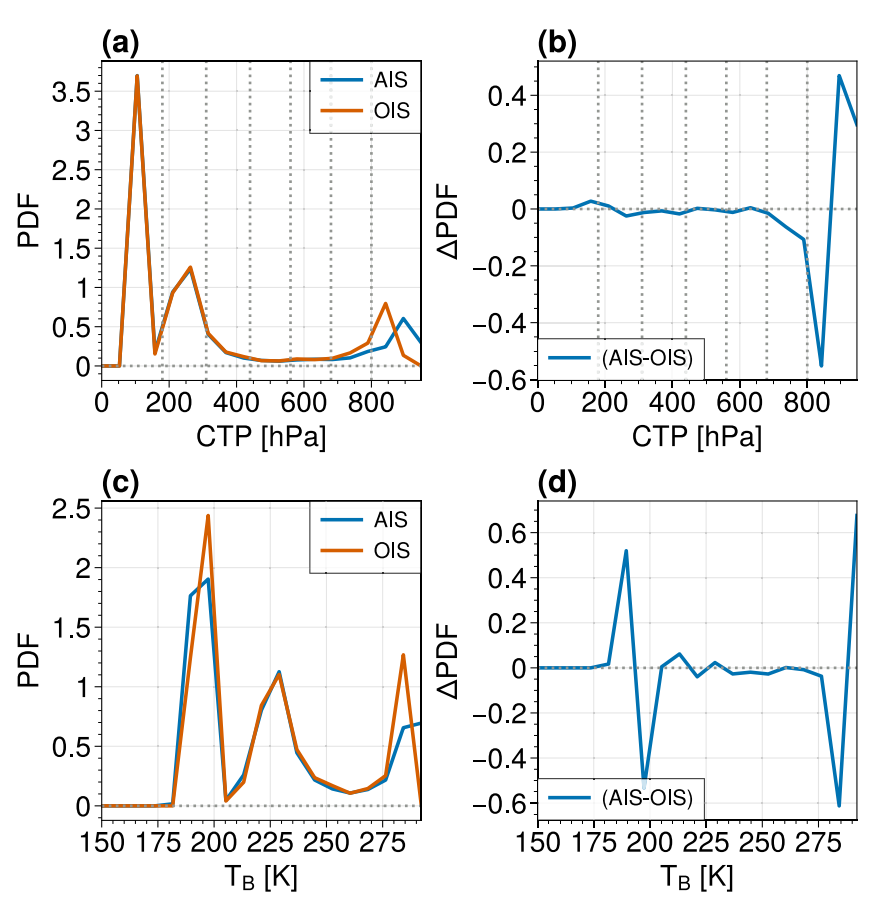


Figure 2. Probability density functions for cloud-top pressure (CTP) (a) and brightness temperature (T_B) (c), where the distribution for the Approximate ISCCP Simulator (AIS) is the blue line and the distribution for the Offline ISCCP Simulator (OIS) is the orange line, and the difference between the AIS and OIS distributions of CTP and T_B (b, d). The vertical dotted gray lines in (a) and (b) are the cutoffs for the International Satellite Cloud Climatology Project bins. The data is from days 1.00–3.75 of a RCE_small 300 K simulation of SAM-CRM-COSP where the 2D output was saved at the same frequency as the 3D output.

of cloud amount occurs in the optically thinnest and highest altitude (the lowest pressure) bin (clouds for $\tau < 0.3$ and CTP < 180 hPa). Similarly, the distribution of clouds with $180 \text{ hPa} \le \text{CTP} < 310 \text{ hPa}$ is consistent across the models, where, as optical thickness increases, cloud amount decreases. For all models except ICON-NWP (and SAM-CRM and MESONH-VERT at 295 K, Figure S1 in Supporting Information S1), the cloud amount in the high-thin regime (clouds with CTP < 310 hPa and τ < 1.6) accounts for over 50% of the cloud amount in the domain, and, for 53% of the models in the 300 K simulation, that regime accounts for over two-thirds of the total cloud amount (37% of models for the 295 K simulations and 63% of models for the 305 K simulations). Figure 4 shows that, except for ICON-NWP and MESONH-VERT (and MESONH), the CRM RCE_small simulations in RCEMIP lack meaningful amounts of low clouds (CTP \geq 680 hPa), which are the stratus- and cumulus-type clouds (Hahn et al., 2001; Rossow & Schiffer, 1991). It is notable that ICON-NWP uses a cloud scheme (which allows for sub-grid scale cloudiness; although this shouldn't impact the cloud condensate, perhaps the interaction within radiation does, for more details see supplement of Wing et al., 2020a); whether this has any explicit impact on the cloud distribution is beyond the scope of this study. MESONH and MESONH-VERT also have a relatively large cloud amount for lower-level clouds (CTP ≥ 310 hPa), which are alto-type and stratus-type clouds (Hahn et al., 2001; Rossow & Schiffer, 1991). SAM-CRM and SAM-CRM-VERT are the models with the lowest total cloud amount (by ~5%-47%), depending on the SST, although $\sim 50\%$ of the models have $\sim 100\%$ cloud amount when the thinnest bin ($\tau < 0.3$) is included.

Figure 5 is similar to Figure 4 except it displays the difference between the ISCCP histograms of the 295 and 305 K simulations (the difference between the 295 and 300 K simulations is shown in Figure S3 in Supporting Information S1 and the difference between the 300 and 305 K simulations is shown in Figure S4 in Supporting Information S1). With warming, the clouds shift upwards from having $180 \text{ hPa} \leq \text{CTP} < 440 \text{ hPa}$ to CTP < 180 hPa

STAUFFER AND WING 6 of 24

19422466, 2023, 11, Downloaded from https://agupubs.onlinelibrary.wiley.com/doi/10.1029/2023MS003738, Wiley Online Library on [05/12/2023]. See the Terms and Conditions (https://on

on Wiley Online Library for rules of use; OA articles are governed by the applicable Creative Commons Licenso

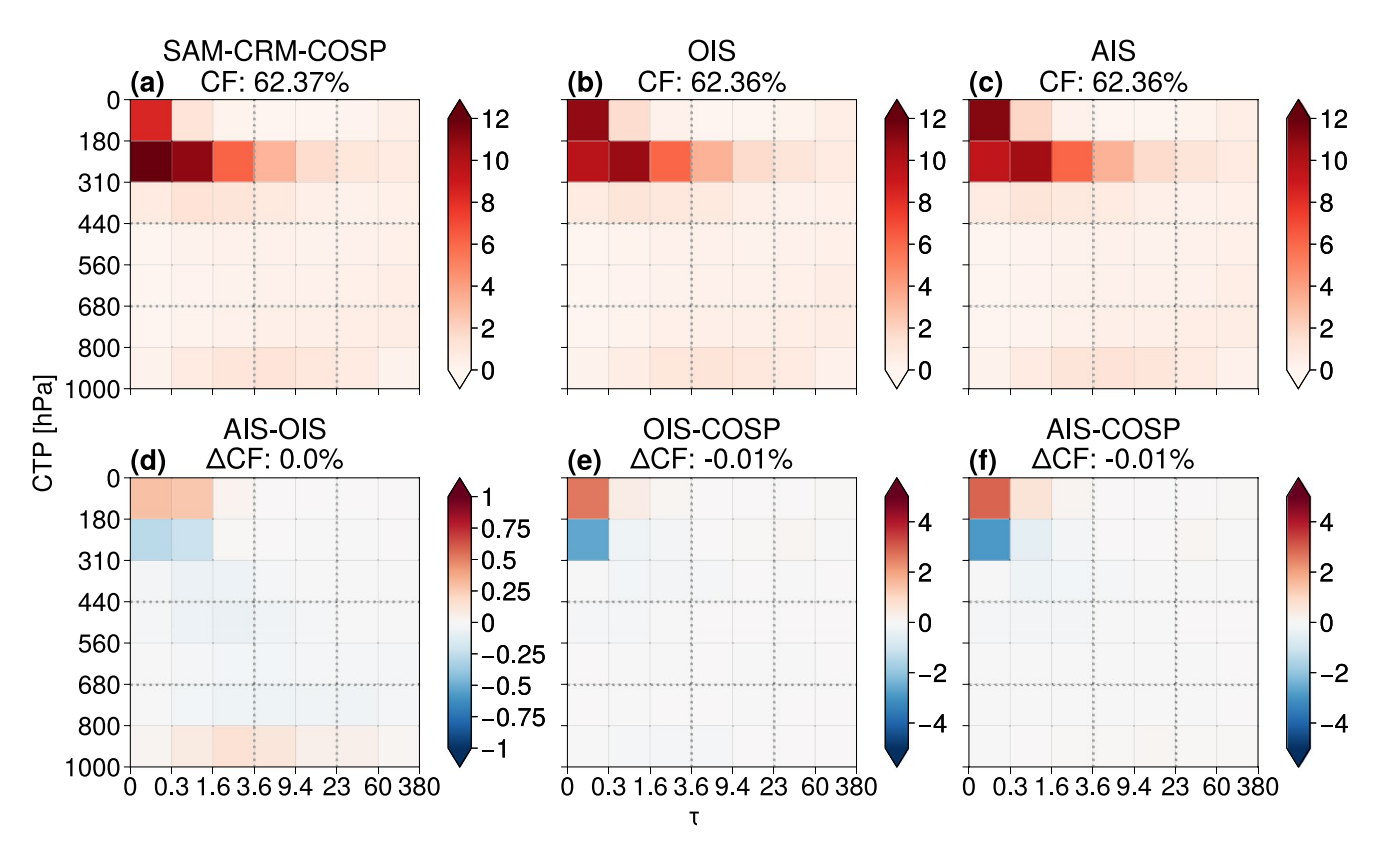


Figure 3. International Satellite Cloud Climatology Project (ISCCP) histograms for the 300 K simulation of SAM-CRM-COSP (a), Offline ISCCP Simulator (OIS) (b), and Approximate ISCCP Simulator (AIS) (c) as well as the difference between the AIS and OIS histograms (d), the difference between the OIS and SAM-CRM-COSP histograms (e), and the difference between the AIS and SAM-CRM-COSP histograms (f). The number at the top of each histogram is the total cloud amount (or the total difference in cloud amount), which is the sum of all the bins in the histogram. The data is averaged over day 75 to the end of the simulation.

(compare the blues in the higher pressure bins to the reds in the lower pressure bin) across all the models. This is consistent with the upward shift in anvil clouds (which would be clouds with CTP < 310 hPa) found in Stauffer and Wing (2022) and expected from physical theory (Hartmann & Larson, 2002; Kuang & Hartmann, 2007). While the majority of the models have a dipole structure that looks like DAM (Figure 5a), some models behave a little differently. For example, the ICON and MESONH family of models (Figures 5e, 5i, 5m, 5l, 5p, and 5q) have an *increase*, rather than a decrease, in medium-thick clouds $(1.6 \le \tau < 9.4)$ for 180 hPa \le CTP < 310 hPa.

The model mean (across RCE_small, RCE_small_vert, and RCE_small_les simulations, Figure 5t) total cloud amount decreases by 2.35% with warming. There is a decrease in total clouds for seven models (36.8% of the models), an increase for three models (15.8%), and a net change of ~0% for nine models (47.4%, however, as seen in Figure S1 in Supporting Information S1, these nine models have 100% cloud amount at 295 K so increasing in cloud amount is not possible to begin with). In Stauffer and Wing (2022), 67% of the RCE_small domain models had anvil cloud fraction that did *not* increase with warming SST (which would be clouds with CTP < 310 hPa), slightly less than the 84% of models that do not have an increase in clouds here. This is because high clouds are not the only clouds being considered in the ISCCP histogram (although high clouds certainly account for the majority of the cloud amount in RCE_small).

4. Cloud Feedback Computation

As in Zelinka et al. (2012a), the cloud feedback calculation requires the use of a cloud radiative kernel (CRK). Since this study uses an idealized framework, which is a distinctly different climate state than that of comprehensive GCMs, the kernels used in Zelinka et al. (2012a) are not used here. Instead, a CRK is created for each model and each SST, individually, with one CRK generated for the entire domain.

To create the kernel, top of atmosphere radiative fluxes are calculated using the RRTMG (Iacono et al., 2008) radiation scheme as interfaced by climlab (Rose, 2018), which requires profiles of cloud liquid and ice water

STAUFFER AND WING 7 of 24

19422466, 2023, 11, Downloaded from https://agupubs.onlinelibrary.wiley.com/doi/10.1029/2023MS003738, Wiley Online Library on [05/12/2023]. See the Terms and Conditions (https://onlinelibrary.wiley.com/terms-and-conditions) on Wiley Online Library for rules of use; OA articles are governed by the applicable Creative Creative Creative Conditions (https://onlinelibrary.wiley.com/terms-and-conditions) on Wiley Online Library for rules of use; OA articles are governed by the applicable Creative Creative Conditions (https://onlinelibrary.wiley.com/terms-and-conditions) on Wiley Online Library for rules of use; OA articles are governed by the applicable Creative Creative Conditions (https://onlinelibrary.wiley.com/terms-and-conditions) on Wiley Online Library for rules of use; OA articles are governed by the applicable Creative Conditions (https://onlinelibrary.wiley.com/terms-and-conditions) on Wiley Online Library for rules of use; OA articles are governed by the applicable Creative Conditions (https://onlinelibrary.wiley.com/terms-and-conditions) on Wiley Online Library for rules of use; OA articles are governed by the applicable Creative Conditions (https://onlinelibrary.wiley.com/terms-and-conditions) on Wiley Online Library for rules of use; OA articles are governed by the applicable Creative Conditions (https://onlinelibrary.wiley.com/terms-and-conditions) on Wiley Online Library for rules of use; OA articles are governed by the applicable Conditions (https://onlinelibrary.wiley.com/terms-and-conditions) on Wiley Online Library for rules of use; OA articles are governed by the applicable Creative Conditions (https://onlinelibrary.wiley.com/terms-and-conditions) on Wiley Online Library for rules of use; OA articles are governed by the applicable Conditions (https://onlinelibrary.wiley.com/terms-and-conditions) on Wiley Online Library for rules of use; OA articles are governed by the applicable Conditions (https://onlinelibrary.wiley.com/terms-and-conditions) on Wiley Online Library for rules of use; OA articles

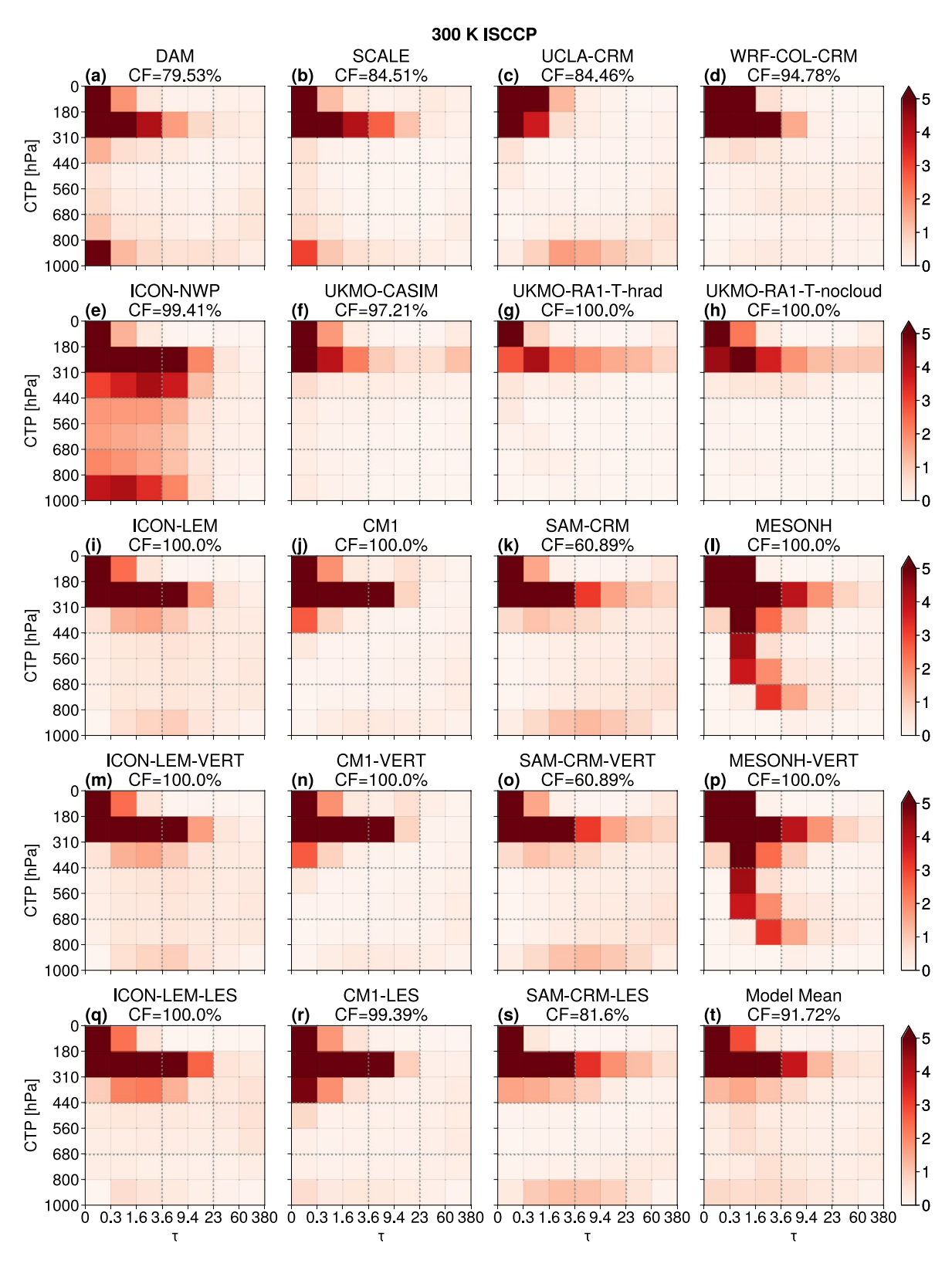


Figure 4. International Satellite Cloud Climatology Project (ISCCP) histograms for the 300 K simulations of RCE_small (a–l), RCE_small_vert (m–p), RCE_small_les (q–s), and the model mean (t). The shading is cloud amount, in percent, binned by cloud-top pressure (hPa, y-axis) and cloud optical depth (x-axis). The number at the top of each histogram is the total cloud amount, which is the sum of cloud amount in all the bins of the histogram.

STAUFFER AND WING 8 of 24

19422466, 2023, 11, Downloaded from https://agupubs.onlinelibrary.viley.com/doi/10.1029/2023MS003738, Wiley Online Library on [05/122023]. See the Terms and Conditions (https://onlinelibrary.viley.com/terms-and-conditions) on Wiley Online Library for rules of use; OA articles are governed by the applicable Creative Commons Licensia

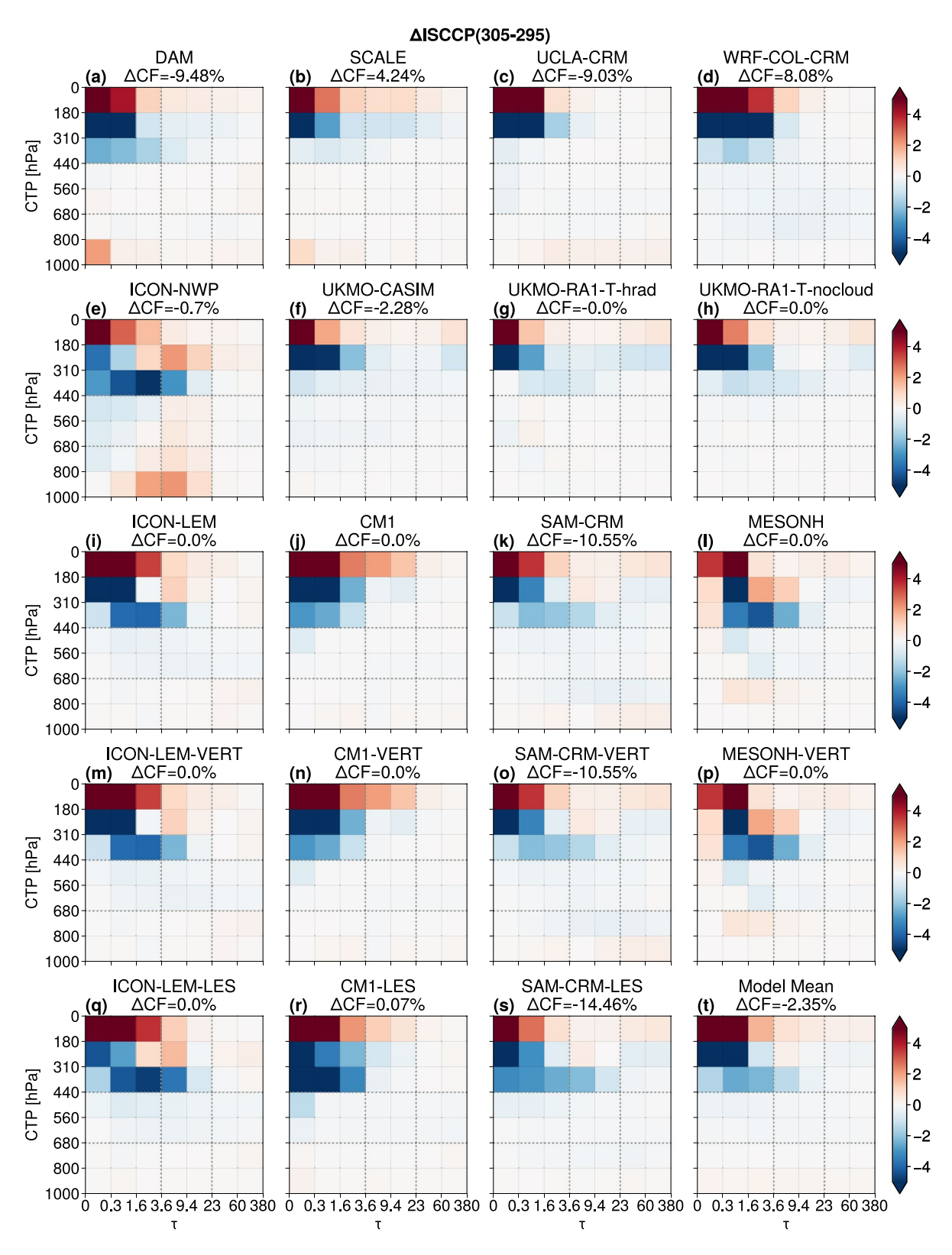


Figure 5. The difference between the 305 and 295 K International Satellite Cloud Climatology Project (ISCCP) histograms of RCE_small (a–l), RCE_small_vert (m–p), RCE_small_les (q–s), and the model mean (t). The shading is the change in cloud amount, in percent, binned by cloud-top pressure (hPa, y-axis) and cloud optical depth (x-axis). The number at the top of each histogram is the total change in cloud amount, which is the sum of cloud amount in all the bins of the histogram.

STAUFFER AND WING 9 of 24

paths, temperature, and trace gases, as well as surface emissivity and albedo properties. The water paths are derived from water content and atmospheric density, using the optical depth parameterizations described in Appendix A, where ice water is identified using the temperature threshold of 260 K. The trace gas profiles use the settings prescribed in the RCEMIP protocol (Wing et al., 2018) and the liquid and ice radii are determined in the same manner as AIS (Appendix A). There is no sub-grid scale cloudiness, a pixel is either cloudy or not cloudy, so the McICA scheme is not implemented. The atmospheric data required from an individual model are domain- and temporally-averaged profiles of temperature and water vapor (specific humidity).

Following Zelinka et al. (2012a), RRTMG is run for the 64 different CTP- τ combinations, where the all-sky kernel has a single-layer cloud placed in the pressure layer given by a particular CTP and cloud water and cloud ice are prescribed by a given τ . The radiative fluxes for the corners of each CTP- τ bin are averaged together to obtain the 49 ISCCP bins. The clear-sky kernel runs RRTMG with cloud liquid water and cloud ice water zeroed out everywhere, from which the all-sky kernel is subtracted to obtain the cloud radiative kernel. This, when divided by 100% in a particular CTP- τ bin, describes the sensitivity of top of atmosphere fluxes due to an increase in cloud amount by 100%.

Figure 6 shows the anomaly from the model-mean net CRK (Figure 6t) for each model, averaged across the three SSTs (Figures S5 and S6 in Supporting Information S1 show the same but for the longwave and shortwave CRKs, respectively). The differences in the CRK between models and SSTs are minor (by much less than 10%) for the majority of models, so this study will use the average net, longwave, and shortwave CRK across models and SSTs (Figure 6t, Figures S5t and S6t in Supporting Information S1, respectively) for all models' cloud feedback computation. While it is technically more accurate to use a unique CRK for each model, using the model-mean CRK ensures that the differences in cloud feedbacks across models result only from differences in the cloud distribution and its changes. Table S1 in Supporting Information S1 shows the model-mean CRK is a representative CRK by comparing the cloud feedbacks of Figures 7a–7e, which uses the model-mean CRK, to those cloud feedbacks using a model's individual CRK.

The kernels are then multiplied by the difference between a warm and cold ISCCP histogram to produce cloud-induced radiative flux anomalies (the net, longwave, and shortwave cloud feedback histograms are shown in Figures S7–S9 in Supporting Information S1, respectively). The cloud feedbacks are decomposed into cloud amount, cloud altitude, cloud optical depth, and residual components, following the modifications of Zelinka et al. (2013) to Zelinka et al. (2012b), described by Equation 1 (Equation B10 of Zelinka et al., 2013):

$$\Delta R_C = K_0 \Delta C_{tot} + \Sigma_{p=1}^P \left(K_p' \Sigma_{\tau=1}^T \Delta C_{p\tau}^* \right)$$

$$+ \Sigma_{\tau=1}^T \left(K_\tau' \Sigma_{p=1}^P \Delta C_{p\tau}^* \right)$$

$$+ \Sigma_{p=1}^P \Sigma_{\tau=1}^T K_R' \Delta C_{p\tau}^*$$

$$(1)$$

where each term describes the cloud amount, cloud altitude, and cloud optical depth, and residual components of the cloud feedback, respectively. The middle two terms on the right-hand side, which represent the cloud altitude and cloud optical depth feedbacks, are multiplying an effective cloud radiative kernel which accounts for variations in either CTP or τ (K'_p and K'_τ , respectively) by the changes in cloud amount at each CTP or τ ($\Delta C^*_{p\tau}$). The first term, the cloud amount feedback, multiplies the cloud radiative kernel weighted by the fraction of cloud amount in each bin (K_0) by the total change in cloud amount. For more details, see Zelinka et al. (2012b, 2013).

Each component describes the cloud feedback arising due to changes in one property (cloud amount, cloud altitude, or cloud optical depth) when the others remain constant. Given the minimal low-cloud amount present in RCE_small simulations (Figure 4), the cloud feedback discussion will focus on the cloud feedbacks considering all the clouds. The further decomposition of the cloud feedbacks into low-clouds (CTP \geq 680 hPa) and non-low clouds (CTP < 680 hPa), following Zelinka et al. (2016) are shown in Figures S10 and S11 in Supporting Information S1, and confirms that the cloud feedbacks in these simulations are dominated by free-tropospheric clouds.

5. Cloud Feedbacks in RCE

The model-mean net cloud feedback is $0.14 \pm 0.20~W~m^{-2}~K^{-1}$ when a large negative outlier (ICON-NWP) is removed; when ICON-NWP is included the net total cloud feedback is $0.09 \pm 0.27~W~m^{-2}~K^{-1}$ (Figure 7a). There are three models (including ICON-NWP) with a negative cloud feedback, averaging $-0.29 \pm 0.21~W~m^{-2}~K^{-1}$,

STAUFFER AND WING 10 of 24

19422466, 2023, 11, Downloaded from https://agupubs onlinelibary.viley.com/doi/10.1029/2023MS003738, Wiley Online Libary on [05/122023]. See the Terms and Conditions (https://onlinelibary.viley.com/terms-and-conditions) on Wiley Online Library for rules of use; OA articles are governed by the applicable Creative Commons Licensea

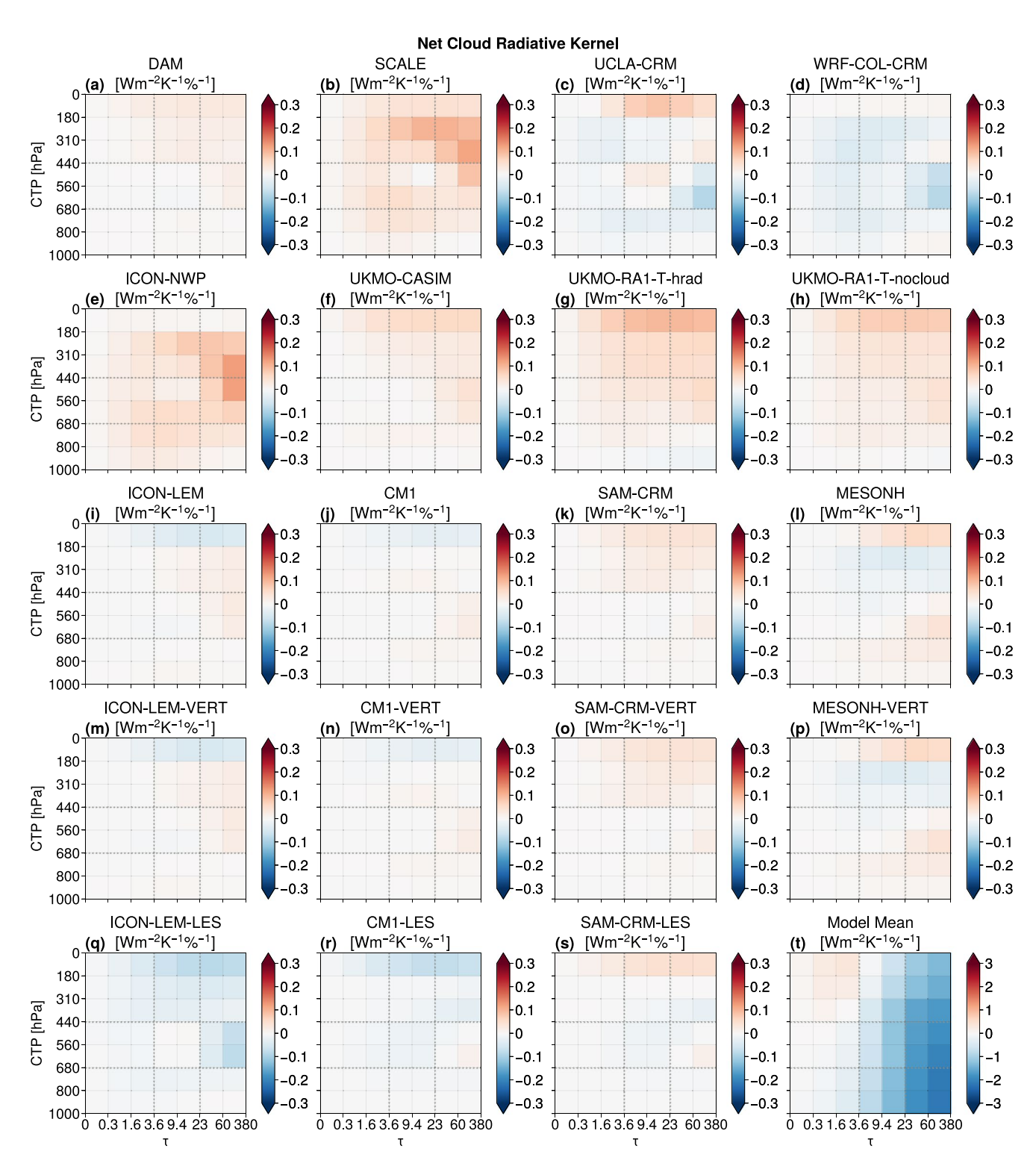


Figure 6. The difference between a model's net cloud radiative kernel (a–s) and the model-mean (t) for RCE_small (a–l), RCE_small_vert (m–p), and RCE_small_les (q–s). All histograms are averaged across the three SSTs. The shading is the change in top of atmosphere net radiative flux due to a 100% increase in cloud amount, in W m^{-2} K $^{-1}$ % $^{-1}$, binned by cloud-top pressure (hPa, y-axis) and cloud optical depth (x-axis). Note: the color bar in panels (a–s) range from -0.3 to 0.3 while panel (t) range from -3 to 3.

STAUFFER AND WING 11 of 24

19422466, 2023, 11, Downloaded from https://agupubs.onlinelibrary.wiley.com/doi/10.1029/2023MS003738, Wiley Online Library on [05/12/2023]. See the Terms and Conditions (https://onlinelibrary.wiley.com/

and-conditions) on Wiley Online Library for rules of use; OA articles are governed by the applicable Creative Commons License

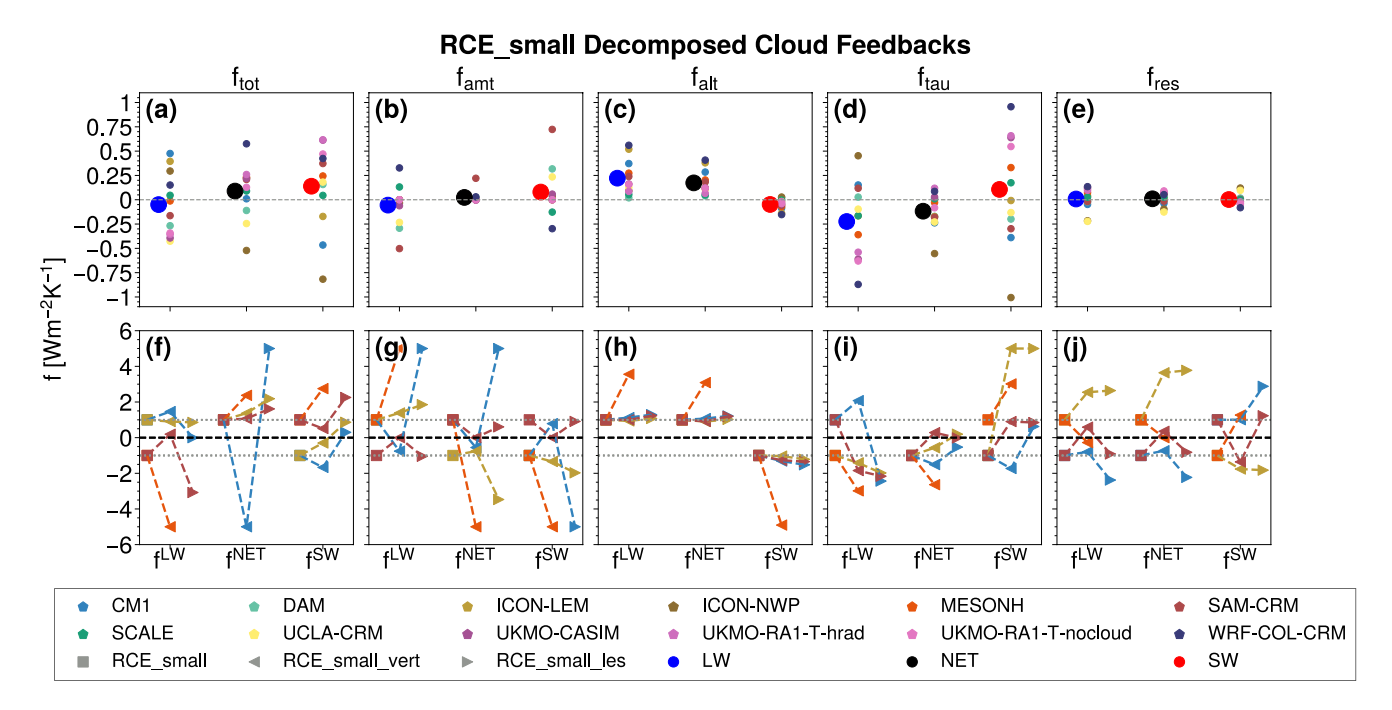


Figure 7. The total cloud feedback (a, f) decomposed into its contributions by cloud amount (b, g), cloud altitude (c, h), and cloud optical depth (d, i), as well as its residual (e, j) following Zelinka et al. (2013). The top row (a–e) contains the cloud feedbacks for RCE_small only, with individual models represented by the smaller symbols, with color varying depending on model. The larger, offset, symbols are the model-mean cloud feedback, whose color represents the radiative flux cloud feedback of that cluster (blue for the longwave cloud feedback, black for the net cloud feedback, and red for the shortwave cloud feedback). The bottom row (f–j) contains the models that have RCE_small_vert (leftward pointed triangle) and/or RCE_small_les (rightward pointed triangle) simulations, as well as the native cloud resolving model (CRM) (square). They are clustered by the radiative flux component of the cloud feedback and normalized by the absolute value of the RCE_small cloud feedback.

and nine models with a positive cloud feedback, averaging 0.22 ± 0.16 W m⁻² K⁻¹. Figure S10 in Supporting Information S1 shows the mean, median, and interquartile range (IQR) of the RCE_small feedbacks. These magnitudes (of both the positive and negative cloud feedbacks) are quite small compared to, for example, the net total cloud feedback value of 0.56 ± 0.36 W m⁻² K⁻¹ found in the CMIP6 models (Table 1), which is up to four times that found in RCE. However, as will be discussed in Section 8, caution must be taken when comparing

Table 1 *RCE-Relevant Cloud Feedback Values* $(W m^{-2} K^{-1})$ *for the Models Assessed in This Study, Those Computed by the CMIP5 and CMIP6 Models as Presented by Zelinka et al.* (2022), and the Expert Assessed Cloud Feedbacks Presented by Sherwood et al. (2020)

	High-cloud altitude	Tropical anvil cloud area	Total cloud
RCE_small ($\tau > 0.0$)	0.20 ± 0.11	-0.07 ± 0.12	0.09 ± 0.27
RCE_small ($\tau > 0.3$)	0.18 ± 0.11	-0.06 ± 0.12	0.05 ± 0.24
CMIP5	0.16 ± 0.10	-0.05 ± 0.05	0.29 ± 0.27
CMIP6	0.23 ± 0.09	-0.03 ± 0.07	0.56 ± 0.36
avg(CMIP5/6)	0.20 ± 0.10	-0.04 ± 0.06	0.46 ± 0.36
Sherwood et al. (2020)	0.20 ± 0.10	-0.20 ± 0.20	0.45 ± 0.33

Note. The definition of the feedbacks in this table are derived from the three decomposed cloud feedbacks following the procedure used for the CMIP models (Zelinka et al., 2022). Values are notated as $\mu \pm \sigma$, where μ is the central value and σ is the uncertainty in the central value using the standard deviation.

the total cloud feedback of RCE to that of comprehensive climate models and, as will be shown, RCE is much more comparable when the appropriate context is given.

ICON-NWP is an outlier due to a large negative shortwave cloud optical depth feedback. This particular model is associated with a relatively significant amount of thin and medium-thick clouds ($\tau < 9.4$) throughout the depth of the troposphere (Figure 4e). ICON-NWP is also the only model with substantial changes in medium-thick clouds for CTP ≥ 440 hPa (Figure 5e). The increase in medium-thick clouds for CTP ≥ 800 hPa (the lowest altitude bin) is especially unique to this model (this feature is also apparent in temporal- and domain-averaged profiles of cloud fraction, where ICON-NWP has a low-level peak in cloud fraction nearly twice the value of the next-highest models, potentially due to the use of a cloud scheme, see Figure 2c of Stauffer & Wing, 2022).

5.1. The Cloud Altitude Feedback

The cloud altitude feedback (Figure 7c) is robustly positive in the longwave, as is expected due to fundamental physical understanding of how cloud altitude changes with warming (for an in-depth review, see Sherwood

STAUFFER AND WING 12 of 24

et al., 2020). High clouds are expected to increase in altitude with nearly isothermal cloud top temperatures or with cloud top temperatures that increase at a rate less than surface warming (Hartmann & Larson, 2002; Kuang & Hartmann, 2007; Zelinka & Hartmann, 2010). In RCEMIP, the increase in anvil cloud altitude with warming SST is the most robust anvil cloud tendency (Stauffer & Wing, 2022), where all models had an increase in anvil cloud altitude and the majority of them did so with a slight increase in anvil cloud temperature. Less longwave radiation is emitted to space than an atmosphere that warms in the upper levels at the same rate as the surface, which would serve as a positive feedback. The shortwave cloud altitude feedback is negative, but with a very small magnitude.

5.2. The Cloud Amount Feedback

The cloud amount feedback (Figure 7b) is a complex feedback consisting of competing longwave and shortwave responses, with a net result near zero, which is consistent with observational constraints (McKim et al., 2023). The inter-model spread for the net cloud amount feedback is small, relative to the longwave and shortwave components (Figure 7b and Figures S10d–S10f in Supporting Information S1). Despite the spread and lack of consensus on a sign for the longwave and shortwave components, the magnitudes still remain equal and near-opposite for most of the models, resulting in the near-cancellation. The mean and IQR across models is negative for the longwave cloud amount feedback and (generally) positive for the shortwave cloud amount feedback (Figures S10d and S10f in Supporting Information S1) arising from the decrease in anvil cloud amount across most models (Stauffer & Wing, 2022). There are two models that have a cloud amount feedback whose sign opposes that of the mean: SCALE and WRF-COL-CRM where the latter is also an outlier as defined as being outside 150% of the IQR (Figures S10d–S10f in Supporting Information S1), due to cloud amount *increasing*, as opposed to decreasing, with warming (Figures 5b and 5d).

5.3. The Cloud Optical Depth Feedback

Finally, in RCE, the cloud optical depth feedback (Figure 7d and Figures S10j–S10l in Supporting Information S1) is the cloud feedback with the largest inter-model spread as well as the largest magnitudes. The model-mean net cloud optical depth feedback is negative, driven by the negative longwave component and offset by the positive shortwave component. This is associated with a general thinning of clouds with warming SST (not shown). There are six models (CM1, DAM, ICON-LEM, ICON-NWP, SAM-CRM, and UCLA-CRM) with shortwave and longwave cloud optical depth feedback signs that are opposite those of the model-mean. This is associated with the distribution of thinner clouds ($\tau < 23$) in those models decreasing with warming, sometimes accompanied by an increase in thicker clouds ($\tau \ge 23$). The reduction in the relative occurrence of thinner clouds implies the clouds are thicker overall, and thus leads to the reduced OLR and absorbed solar radiation. These models behave in a way such that the strength of the shortwave component overpowers the longwave component, recovering a negative net cloud optical depth feedback, the same sign as the model-mean. Four models (SCALE, UKMO-CASIM, UKMO-RA1-T-hrad, and WRF-COL-CRM) have a positive net cloud optical depth feedback (opposite of the model-mean), despite the signs of the longwave and shortwave components following that of the model-mean, due to the strength of the shortwave component.

5.4. The Cloud Feedback Residual

The residuals (Figure 7e) are generally small and, on average, slightly positive in the longwave and net and near-zero in the shortwave. For most models, the decomposed cloud feedbacks have an associated residual that is less than a third of the respective decomposed and total cloud feedbacks. The average residual is $\sim \pm 0.05$ W m⁻² K⁻¹ with an inter-model spread extending to $\sim \pm 0.2$ W m⁻² K⁻¹, which is similar to the residuals found in a similar decomposition for CFMIP1, which had a model mean of less than 0.1 W m⁻² K⁻¹ and a model spread extending to $\sim \pm 0.25$ W m⁻² K⁻¹ (Zelinka et al., 2016).

STAUFFER AND WING 13 of 24

6. Sensitivities of the Cloud Feedback

6.1. Base Temperature Dependence

Section 5 discussed the cloud feedback from 295 to 305 K; the sensitivity of the cloud feedback to different base surface temperatures can be looked at by analyzing the cloud feedbacks from 295 to 300 K and 300 to 305 K, separately (Figure S11 in Supporting Information S1). The model-mean and inter-model spread of the cloud feedbacks for each $\Delta 5$ K warming are comparable to each other and that of the $\Delta 10$ K warming with no stand out features that would imply differing sensitivity of the cloud response to warming SST with a warmer base state. Put differently, there is no temperature with a stronger feedback; it depends on the individual cloud regime and flux component, but, in the net, the cloud feedbacks are equal across the warming ranges. The inter-model spread for a given $\Delta 5$ K cloud feedback is similar to the $\Delta 10$ K, although sometimes, but not always, the spread can be higher for the larger temperature range.

6.2. Model Resolution Dependence

Despite the higher resolution of CRMs being a step-up from GCMs, there are still parameterizations that, on the finer scale, play important roles in various cloud regimes, especially low clouds. For example, as overviewed by Cronin and Wing (2017), CRMs still have to parameterize some processes, such as turbulence (Romps, 2014). RCEMIP has the advantage of containing a few models that have simulations with higher resolutions in both the vertical (RCE_small_vert) and horizontal (RCE_small_les). Figures 7f-7j shows the decomposed cloud feedbacks for the four models that have these higher resolution versions. Note: each cloud feedback for a set of RCE_small, RCE_small_vert, and RCE_small_les simulations is normalized by the absolute value of the cloud feedback associated with the respective RCE_small value such that if, for example, a RCE_small_les model has a value greater than one, then that model has a positive cloud feedback whose magnitude is greater than that of the RCE_small model associated with the RCE_small_les model. The cloud feedbacks associated with RCE_small will be ±1, by definition, depending on the sign of the feedback.

The net total cloud feedback (Figure 7f) increases in magnitude with finer horizontal grid spacing (RCE_small to RCE_small_vert) and finer vertical grid spacing (RCE_small_vert to RCE_small_les), alike, for all models except CM1. When considering the effects of the longwave and shortwave total cloud feedbacks, the magnitude for those in CM1 and MESONH increases with finer horizontal grid spacing and the total cloud feedbacks for CM1 changes sign for finer vertical grid spacing. ICON-LEM, on the other hand, has a total cloud feedback whose magnitude decreases with finer horizontal grid spacing and either has a reduced magnitude (in the longwave) or changes sign (in the shortwave) for finer vertical grid spacing. The total cloud feedback in SAM-CRM changes sign with finer horizontal and vertical grid spacing in the longwave while, in the shortwave, the magnitude reduces for finer horizontal and vertical grid spacing.

The cloud altitude feedback (Figure 7h) robustly increases in magnitude for finer vertical grid spacing (RCE_small_vert to RCE_small_les). The same occurs for the cloud feedbacks in MESONH and CM1 with for finer horizontal grid spacing (RCE_small to RCE_small_vert), but the cloud altitude feedback in SAM-CRM and ICON-LEM both have a reduced magnitude for finer horizontal grid spacing (for the longwave and net cloud altitude feedbacks, only).

The cloud amount feedback (Figure 7g) is zero for all models except the SAM-CRM family (and CM1-LES, but with magnitudes much less than that found in the SAM-CRM family). Those models all have a net-zero change in cloud amount with warming SST (Figures 5i, 5j, 5l, 5m, 5n, 5p, 5q, and 5r) due to the cloud amount being over 99% at all SST (Figures 4i, 4j, 4l, 4m, 4n, 4p, 4q, and 4r, Figures S1i, S1j, S1l, S1m, S1n, S1p, S1q, S1r, S2i, S2j, S2l, S2m, S2n, S2p, S2q, and S2r in Supporting Information S1). Cloud amount in SAM-CRM, on the other hand, is well below 100% (Figures 4k, 4o, and 4s, Figure S1k, S1o, S1s and S2k, S2o, S2s in Supporting Information S1) and decreases by 10.55% from 295 to 305 K for the RCE_small and RCE_small_vert simulations and decreases by 14.46% for the RCE_small_les simulation (Figures 5k, 5o, and 5s). For SAM-CRM, the magnitude of the cloud amount feedback reduces to near-zero with finer horizontal grid spacing (i.e., SAM-VERT has a cloud amount feedback near-zero). The cloud amount feedback in SAM-LES shares a sign with SAM-CRM, but with a reduced magnitude in the net and shortwave, and a larger magnitude in the longwave.

STAUFFER AND WING 14 of 24

19422466, 2023, 11, Downloaded from https://agupubs.onlinelibrary.wiley.com/doi/10.1029/2023MS003738, Wiley Online Library on [05/12/2023]. See the Terms and Conditional Conditional Conditions of the Conditional Conditiona

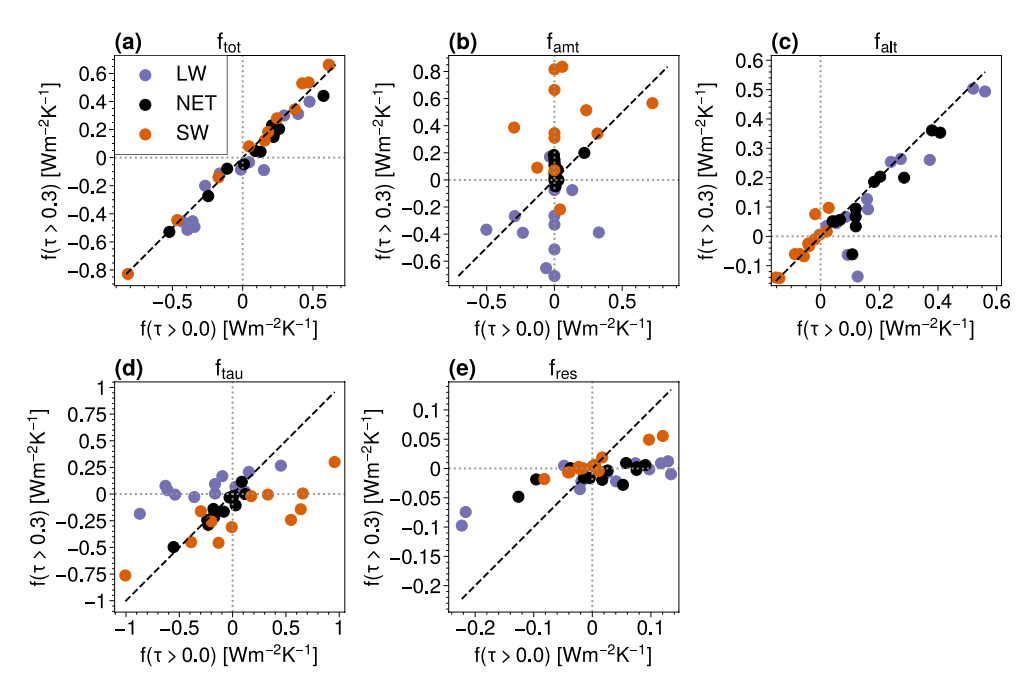


Figure 8. The decomposed cloud feedbacks excluding the thinnest optical depth bin plotted against the cloud feedbacks including the thinnest optical depth bin. Each circle is a different model, the blue circles are the longwave cloud feedbacks, the black circles are the net cloud feedbacks, and the orange circles are the shortwave cloud feedbacks. The black dashed line is the one-to-one line. Note: the axis ranges differ across the panels.

The net cloud optical depth feedback (Figure 7i) increases in magnitude for CM1 and MESONH, reduces in magnitude for ICON-LEM, and switches sign for SAM-CRM with finer horizontal grid spacing (RCE_small to RCE_small_vert). The sign switches for finer vertical grid spacing (RCE_small_vert to RCE_small_les) for ICON-LEM and SAM-CRM, while the magnitude of the net cloud optical depth feedback decreases for finer vertical grid spacing for CM1. In the longwave, the cloud optical depth feedback for all models except SAM-CRM (which switches sign) increases in magnitude for finer horizontal grid spacing while increasing in magnitude with finer vertical grid spacing for all but CM1 (which switches sign). The shortwave cloud optical depth feedback for CM1 and MESONH increase in magnitude while it switches sign for ICON-LEM and SAM-CRM. The shortwave cloud optical depth feedback does something different for each model for finer vertical grid spacing.

Ultimately, an increase in horizontal resolution results in a more positive cloud feedback in the shortwave (which drives the net cloud feedback response) and a more negative cloud feedback in the longwave. For most models, this is driven primarily by the cloud optical depth feedback response to finer grid spacing due to the minimal changes in the cloud altitude feedback and the near-zero cloud amount feedback. For the most part, the temperature sensitivity of the cloud feedbacks is similar to that discussed for the CRMs only in Section 5, especially for RCE_small_les (Figure S12 in Supporting Information S1, right column). For RCE_small (Figure S12 in Supporting Information S1, middle column), there are instances where at least one of the components of the cloud feedback has an opposing sign for one or both of the $\Delta 5$ K cloud feedbacks compared to the $\Delta 10$ K cloud feedbacks.

6.3. Handling the τ < 0.3 Bin

The optically thinnest clouds are often excluded when computing total cloud fraction from ISCCP histograms because they are not well observed by ISCCP and they are assumed to be radiatively irrelevant. As evident in Figure 6, the radiative flux sensitivity to cloud changes for $\tau < 0.3$ is near zero. However, since these simulations produce so many thin clouds, the assumption that they are not relevant is re-examined, and the sensitivity of the cloud feedbacks to the inclusion or exclusion of that bin is tested. For over 80% of the models, more than a third of the total cloud amount occurs in the $\tau < 0.3$ bin (for over 50% of the models, the net cloud

STAUFFER AND WING 15 of 24

feedback in the thinnest bin is less than a third of the total net cloud feedback. There are only two models whose cloud feedback in the thinnest bin contributes more than the rest of the histogram to the total net cloud feedback (SCALE and UKMO-RA1-T-nocloud). Although the impact of including the $\tau < 0.3$ appears to be small, understanding the impact of the thinnest clouds on the decomposed cloud feedbacks warrants further attention.

Figure 8 shows the cloud feedback components when the thinnest optical thickness bin is excluded against the cloud feedbacks when the thinnest optical thickness bin is included. The thinnest optical depth bin primarily affects the cloud amount and cloud optical depth feedbacks (Figures 8b and 8d). When the thinnest bin is excluded, the magnitude of the cloud amount feedback (Figure 8b) tends to be larger than when it is included (the shortwave cloud amount feedback is more positive and the longwave cloud amount feedback is more negative). Conversely, for the cloud optical depth feedbacks (Figure 8d), the magnitudes are reduced when the thinnest bin is excluded (the shortwave cloud optical depth feedback is less positive and the longwave cloud optical depth feedback is less negative). In some cases, the sign reverses (in both the longwave and shortwave). However, the opposing signs (and somewhat equivalent changes in magnitude) of the shortwave and longwave components cancel for the net cloud optical depth feedbacks. Similarly, the total cloud feedback (Figure 8a) is largely unaffected by whether or not the $\tau < 0.3$ bin is included in the calculation because the impact on the cloud amount and cloud optical depth feedbacks are near-equal and opposite, although we acknowledge this may be a consequence of the overall cloud optical depth thinning with warming. The magnitudes of the total cloud feedback are slightly enhanced when the thinnest bin is included, but nowhere near the magnitude of the changes seen in the cloud amount and cloud optical depth feedbacks.

It is reassuring, however, that these sensitivities are most prevalent in the components of the cloud feedbacks that are impacted by the baseline amount of clouds present (the cloud amount and cloud optical depth feedbacks). Even though the decomposition isolates contributions due to changes in, for example, cloud optical depth from changes in cloud altitude and cloud amount, it does not imply that the baseline amount of clouds wouldn't impact the cloud optical depth feedback. More clouds means reduced transmission (or enhanced reflection) of radiation through the atmosphere in general. If the only anticipated impact to cloud feedbacks by the inclusion of this thinnest bin would be to those components affected by baseline cloud amount, then the cloud altitude feedback should be largely unaffected by this bin, which is, indeed, what occurs (Figure 8c).

To test the performance of cloud identification using ISCCP procedures, the cloud amount identified by ISCCP is compared to cloud amount as defined by a total cloud water threshold. Following the definition for cfv2 from Stauffer and Wing (2022), cloud fraction is defined as the fraction of columns in the horizontal domain that has at least one pixel in its column with total cloud water content exceeding 10^{-5} gg⁻¹. Figure 9 shows the sum of the ISCCP histogram (total cloud amount), including and excluding $\tau < 0.3$, regressed against the cloud fraction of the domain as defined using the total cloud water threshold. When the $\tau < 0.3$ bin is removed, the cloud amount, as defined by cfv2, is almost perfectly recovered by the sum of the ISCCP histogram (the orange regression line is almost perfectly over-laid upon the black one-to-one line) with correlation coefficients greater than 0.9 for all models, except MESONH and MESONH-VERT.

On average, across the models, the sum of the ISCCP histogram (i.e., the total cloud fraction) excluding the $\tau < 0.3$ bin is ~45% of the histogram sum including the bin (Figure 9p), across the three SSTs. The total cloud feedback when the $\tau < 0.3$ bin is excluded is itself, on average, within 20% of the total cloud feedback including that bin (not shown). Despite the cloud distribution primarily being contained in the high and thin bins, we have confirmed that these clouds are mostly radiatively irrelevant and excluding them does not qualitatively change any of the results. This also gives somewhat a posteriori, and radiation-based, evidence for the choice of cfv2 and exclusion of saturation mixing ratio over water in the definition of a cloud (compared to the original cloud fraction definition; Stauffer & Wing, 2022). Future work may consider whether the production of an abundance of high, thin clouds by CRMs in RCE is realistic or an artifact of the RCE state and a bias of CRMs. Nevertheless, even if the radiative impact of the thinnest bin is small, the abundance in these simulations suggests that the impact may not be negligible. Indeed, although the general conclusions, especially for the total cloud feedback, remain unchanged, there are small impacts to the components of the cloud feedback and, thus, the decision to include the optically thinnest bin in the cloud feedbacks computed throughout this study.

STAUFFER AND WING 16 of 24

19422466, 2023, 11, Downloaded from https://agupubs onlinelibary.wiley.com/doi/10.1029/2023MS003738, Wiley Online Library on [05/12/2023]. See the Terms and Conditions (https://onlinelibrary.wiley.com/terms-and-conditions) on Wiley Online Library for rules of use; OA articles are governed by the applicable Creative Commons Licensea

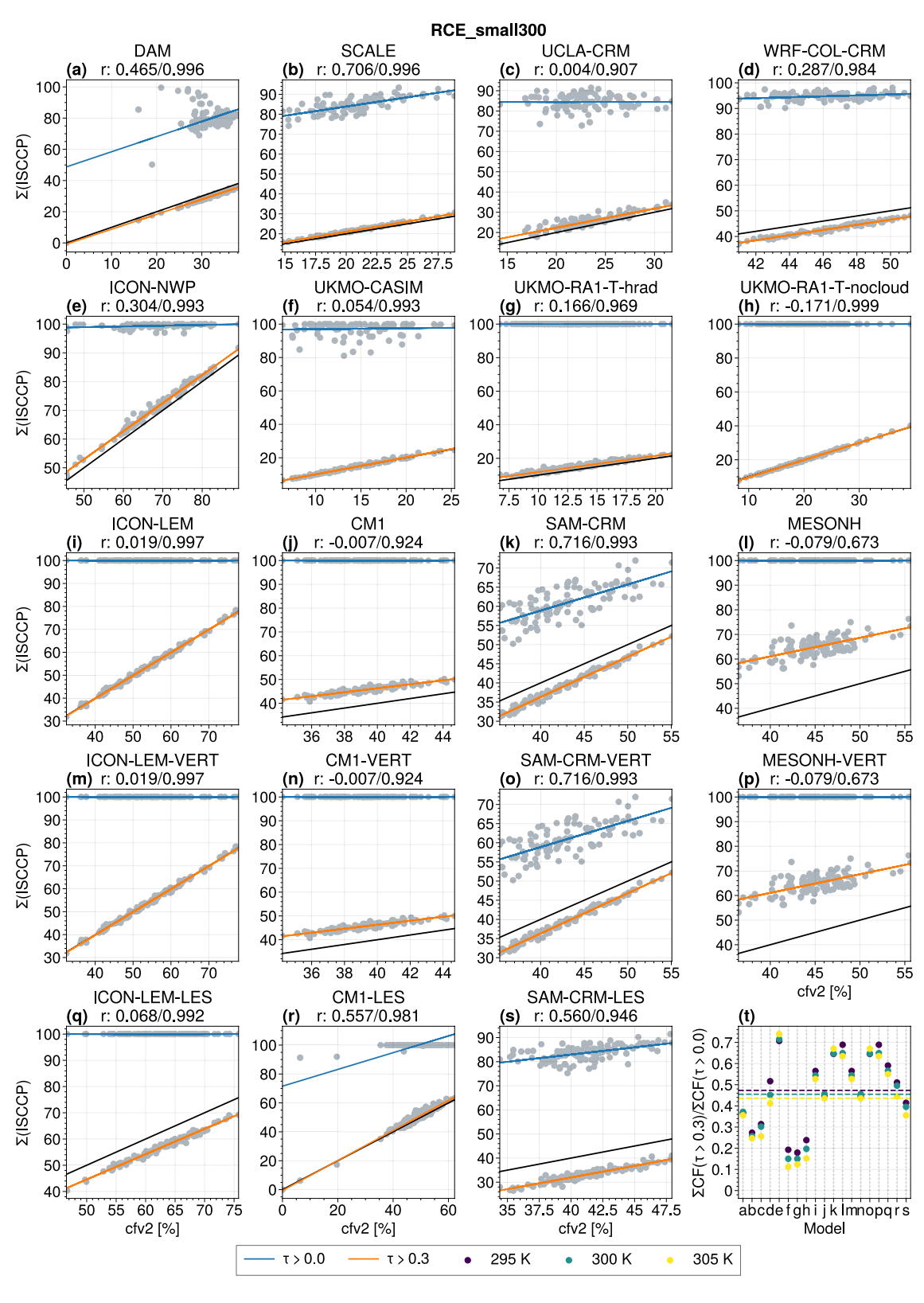


Figure 9.

STAUFFER AND WING 17 of 24

19422466, 2023, 11, Downloaded from https://agupubs.onlinelibrary.wiley.com/doi/10.1029/2023MS003738, Wiley Online Library on [05/12/2023]. See the Terms and Conditions (https://online

on Wiley Online Library for rules of use; OA articles are governed by the applicable Creative Comm

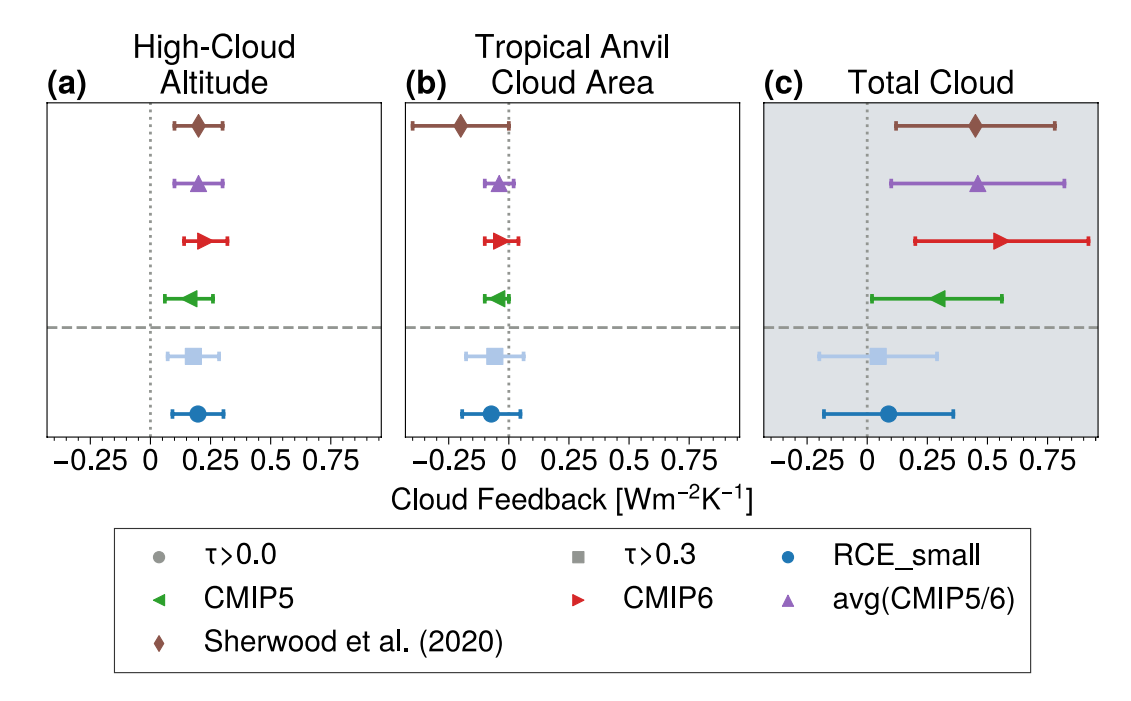


Figure 10. RCE-relevant decomposed cloud feedbacks for the RCE_small simulations including and excluding $\tau < 0.3$ (the values below the gray dashed line) as well as the cloud feedbacks for CMIP5, CMIP6, and the average of CMIP5 and CMIP6 (Zelinka et al., 2022), and the expert assessed cloud feedbacks (Sherwood et al., 2020). The scatter is the central value while the uncertainty bars demarcate $\pm \sigma$. The total cloud feedback is shaded gray to differentiate from the other cloud feedbacks because radiative-convective equilibrium does not include clouds such as land and arctic that are included in the CMIP and expert assessed values.

7. Discussion

Thus far, the focus was on describing the cloud feedbacks in RCE following their categorization into components due to changes in cloud amount, cloud altitude, and cloud optical depth (Schneider & Dickinson, 1974). But how do cloud feedbacks in RCE_small compare to those in realistic, comprehensive GCM simulations and expert assessment from multiple lines of evidence (such as in Sherwood et al., 2020)?

Great care has to be taken when comparing cloud feedbacks in RCE to cloud feedbacks derived in the CMIP models or expertly assessed by multiple lines of evidence due to the limitations of the applicability of RCE. As discussed in Section 1, RCE is not applicable to the middle-high latitudes or land regions, nor does it simulate stratocumulus clouds. Of the seven cloud feedbacks assessed in Sherwood et al. (2020), two can be assessed in the RCEMIP simulations examined here in the same manner as applied to GCMs by Zelinka et al. (2022). These cloud feedbacks include the high-cloud altitude feedback and the tropical anvil cloud area feedback (the sum of high-cloud amount and optical depth feedbacks). While the high-cloud altitude feedback is averaged globally in Sherwood et al. (2020) and Zelinka et al. (2022), the RCE version (which is representative of the tropics only) is still considered, especially given how strongly the tropical region contributes to this feedback and regime of clouds. Similarly, although the total cloud feedback cannot be directly compared since RCE is missing a significant amount of cloud types and regions, the tropics contribute a significant amount to the total cloud feedback (Sherwood et al., 2020) and, as such, RCE has the potential to add some insight. The value of these feedbacks as assessed by Sherwood et al. (2020, their Table 1), computed by CMIP5 and CMIP6 (Table 3 of Zelinka et al., 2022), and in RCE_small are listed in Figure 10 (and Table 1).

Figure 9. Sum of the International Satellite Cloud Climatology Project (ISCCP) histogram including and excluding the thinnest optical depth bin plotted against the fraction of the domain that has at least one cloudy level, where a cloud is defined by cfv2 in Stauffer and Wing (2022) for each model's 300 K simulation (a–s). Individual circles are the sum of the histogram for each time step, the blue line is the regression line for $\tau > 0.0$ versus cfv2, the orange line is the regression line for $\tau > 0.3$ versus cfv2, and the black line is the one-to-one line. The numbers at the top of the panels are the correlations of the blue line and orange line from left to right. The ratio of the temporally-averaged ISCCP sum excluding the thinnest bin to that including the thinnest bin is in panel (t) for each sea surface temperature (the different colors). The x-axis is the ratio for each model, where the model is denoted by a letter which corresponds to the individual model's panel (a–s).

STAUFFER AND WING 18 of 24

The model-mean value of the high-cloud altitude feedback (Figure 10a) in RCE_small, and its uncertainty, is well-matched with the values obtained from multiple lines of evidence (Sherwood et al., 2020), which includes those calculated by GCMs. This lends confidence in using RCE as a tool in studying cloud feedbacks derived in this manner with the benefit of having multiple models with higher resolutions and explicit representation of convection and as a way to expand understanding of deep-convective contributions to the cloud feedback.

The tropical anvil cloud area feedback (Figure 10b) in RCE_small, on the other hand, has a central value within the uncertainty range for the CMIP values (on the high end of the range) as well as the expert assessment (on the low end) but its own uncertainty range expands well outside the bounds of the CMIP models. In particular, the RCE_small estimates do not rule out a positive tropical anvil cloud area feedback.

When considering only the population of models which have a RCE_small simulation and a higher resolution companion (RCE_small_vert or RCE_small_les), the story is a little different. Figure S13 in Supporting Information S1 is a version of Figure 10 but only for these models. Generally, the model-mean cloud feedbacks of the higher resolution models are within the spread of RCE_small, except for the tropical anvil cloud area feedback which is, instead, slightly *positive* for the RCE_small_les simulations. This is opposite to prior estimates (Sherwood et al., 2020; Zelinka et al., 2022) and indicates that the tropical anvil cloud area feedback is sensitive to resolution. Another distinction is the spread in the RCE_small_vert models, which is larger than that of RCE_small or RCE_small_les.

The total cloud feedback is also included (Figure 7c and Figure S13c in Supporting Information S1) which, for the expert assessment and CMIP, is simply the sum of all six cloud feedbacks assessed by Sherwood et al. (2020) while for the RCE_small models, the total cloud feedback as presented in Section 5 is used (also Figure 7a). As discussed above, the total cloud feedback in RCE is not directly comparable to a global mean total cloud feedback in realistic simulations. The total cloud feedback used for RCE_small is also not obtained in the same manner as done for CMIP. However, it is included here as a number of interest. The spread in RCE_small is considerable and spans both positive and negative values with a central value much less than prior studies. Remarkably, however, when only considering the population of models with increased horizontal or vertical resolution (Figure S13c in Supporting Information S1), the total cloud feedback statistics become more comparable to prior studies, especially for RCE_small_les (although there are only three models considered here). These central values and the majority of the spread still favor the low end of the spread in the prior studies.

Cloud feedbacks in RCE simulations should not be expected to be comparable to global averages in CMIP due to the restricted cloud and climate representation. However, the remarkably similar central value and spread of the cloud feedbacks between the two simulation types reflects not only the important contribution of tropical deep-convective clouds to the total global cloud feedback, but also the power and capability such a simplified framework of a single segment of Earth presents in RCE simulations. This framework gets relatively close to recovering the total global cloud feedback by *just* considering the behavior of tropical deep-convective clouds.

8. Conclusion

In RCEMIP, we found that the net total cloud feedback is, on average, positive, in which the longwave cloud altitude feedback is the single most positive contributor. The cloud amount and cloud optical depth feedbacks have substantial cancellation between their longwave and shortwave components, where the net cloud amount feedback is near zero (both on average and in most individual models) and the net cloud optical depth feedback is on average negative. Note, even though the inter-model mean net total cloud feedback is positive, several individual models have negative net total cloud feedbacks.

The cloud altitude feedback exhibits the best agreement across models and is the sole positive contributor to the longwave total cloud feedback. This is due to a robust (and expected) increase in cloud altitude accompanied by a cloud top temperature increase rate lower than that of surface warming. Decreases in cloud amount result in competing longwave and shortwave components of the cloud amount feedback to make the net cloud amount feedback near-zero with minimal inter-model spread relative to the shortwave and longwave components. The cloud optical depth feedback, on the other hand, has the largest magnitudes and inter-model spread and is, on average, slightly negative in the net, driven by the negative longwave component that accompanies cloud thinning with warming SST.

The central value and spread of the high-cloud altitude feedback for the RCE_small simulations is well-matched with prior work (Figure 10a, Table 1), which lends confidence in the computation of cloud feedback components

STAUFFER AND WING 19 of 24

in this manner. The tropical anvil cloud area feedback has contributions from two components of the total cloud feedback associated with considerable inter-model spread in RCE_small. Nevertheless, the central value is negative and comparable to that found using GCMs and is within the spread of the assessment incorporating multiple lines of evidence. However, there are a few models with positive tropical anvil cloud area feedbacks; in particular, the LES models with finer horizontal grid spacing. And, although the total cloud feedback in RCE_small is not obtained in the same way as prior work, the results of RCE_small lends increased emphasis on the importance of tropical convection to the understanding of the total cloud feedback.

It is important to note that the cloud feedbacks studied here are assessed in RCE_small simulations that do NOT exhibit convective organization, which is present in the real tropics (e.g., Holloway et al., 2017; Houze, 2004), modulates the observed tropical radiation budget (Bony et al., 2020), and could thus potentially influence the value of the cloud feedbacks (e.g., Cronin & Wing, 2017). A subsequent paper will introduce the cloud feedback decomposition of the RCE_large CRM simulations in RCEMIP (in which convection aggregates and impacts the mean climate state). This will be compared to the cloud feedbacks in a GCM to assess the influence of explicit versus parameterized convection in a RCE setting. The RCEMIP cloud feedbacks will also be contextualized by comparing them to results from simulations higher up in the model hierarchy, including a GCM aquaplanet simulation from CFMIP3 (Webb et al., 2017) as well as other configurations of RCE such as a RCEMIP GCM and RCE simulations that introduce an SST gradient. Although further details are reserved for that paper, RCE_large simulations have a much more realistic distribution of clouds within their ISCCP histograms, including the introduction of a low cloud regime. Using the results from this paper as a starting point, the subsequent paper will aim to not only determine the cloud feedback in an increasingly realistic environment (while maintaining the advantage of explicit convection), but will also assess the impact of organized convection on the cloud feedback.

Appendix A: Offline ISCCP Simulator

The primary processes that are derived are (a) a parameterization for cloud optical depth (both liquid and ice) and (b) brightness temperature from which CTP is derived. The calculation of brightness temperature (in the infrared) and the corresponding cloud top temperature mostly follows the procedures of Klein and Jakob (1999) and Webb et al. (2001) and are reviewed here, for clarity.

Cloud ice optical depth (in the visible band) is defined by Equation A1:

$$\tau_i = IWP(a_0 + a_1/D_{ge}) \tag{A1}$$

where $a_0 = -0.291721 \times 10^{-4} \,\mathrm{m}^{-1}$ and $a_1 = 2.51925$ (from Equation 3.9a and Table 3a of Fu, 1996) and IWP is vertically resolved ice water path. Cloud liquid optical depth is defined by Equation A2:

$$\tau_l = LWP(a_i + b_i/R_{eff}) \tag{A2}$$

where $a_i = 2.817 \times 10^{-2}$ m²/g and $b_i = 1.305 \, \mu \text{m}^2/\text{g}$ (from Equation 1 and Table 1 of Slingo, 1989) and LWP is vertically resolved liquid water path. Ice (D_{ge}) and liquid (R_{eff}) effective radii are computed as in SAM-CRM (Khairoutdinov & Randall, 2003), where R_{eff} is a constant equal to 14 μ m and D_{ge} is a set profile of ice radii defined by Kiehl et al. (1998).

These definitions are constant across all models and are therefore independent of the atmosphere of a particular simulation, potentially differing from a model's online calculations of cloud optical properties if their native implementation uses different parameterizations.

The top of atmosphere radiance includes contribution from each level as well as the surface, defined by Equation A3 (Equation A4 of Klein & Jakob, 1999):

$$F_{TOA} = \sum_{nlev}^{i} t^{i} \epsilon^{i} BB(T^{i}) + t^{sfc} \epsilon^{sfc} BB(T^{sfc})$$
(A3)

STAUFFER AND WING 20 of 24

19422466, 2023, 11, Downloaded from https://agupubs.onlinelibrary.wiley.com/doi/10.1029/2023MS003738, Wiley Online Library on [05/12/2023]. See the Terms and Condition of the C

) on Wiley Online Library for rules of use; OA

articles are governed by the applicable Creative Commons License

$$t^{i} = \prod_{j=TOA}^{i-1} 1 - \epsilon^{i} \tag{A4}$$

and longwave emissivity is computed from the total visible cloud optical depth, defined by Equation A5:

$$\epsilon = 1 - \exp(-(\tau_i + \tau_l)) \tag{A5}$$

BB is a quantity proportional to blackbody emission at 11 μm, defined by Equation A6 (Equation A5 of Klein & Jakob, 1999):

$$BB = (\exp(1,307.27/T^{i}) - 1)^{-1}.$$
 (A6)

Partial transmission through clouds is accounted for by including the surface emission that is transmitted through a cloud, defined by Equation A7 (Equation A9 of Klein & Jakob, 1999):

$$BB(T_{cld}) = (F_{TOA} - (1 - \epsilon_{cld}) * \epsilon_{sfc} * BB(T_{sfc})) / \epsilon_{cld}$$
(A7)

where ϵ_{sfc} = 0.99 and ϵ_{cld} uses the longwave-adjusted cloud optical depth described by Equation A8 (from Equation A8 of Klein & Jakob, 1999):

$$\epsilon_{cld} = 1 - \exp(-(\tau_i + \tau_l)/2.13).$$
 (A8)

Brightness temperature for a clear-sky column ($\tau \le 10^{-7}$) is found using Equation A6 where BB is set to the top of atmosphere irradiance found by Equation A3 while brightness temperature for a cloudy column ($\tau > 10^{-7}$) is found using Equation A7. Cloud top pressure is simply the pressure interpolated from the layer of the troposphere where the temperature is closest to the cloud top temperature.

The limitations of ISCCP retrievals in the original design of the simulator (Klein & Jakob, 1999; Webb et al., 2001) remain, such as the limits of the CTP and τ resolutions and the CTP estimation in a column associated with the highest (the lowest pressure) clouds masking changes in clouds below this level. Although left for future work and implementation, restricting the analysis to these bins simply to mimic the resolution limitations of the ISCCP instruments may not be necessary and, going forward, other radiatively-relevant properties and resolutions of data could be considered when calculating and decomposing the cloud feedback. Finally, we note that one major difference between the simulator here and the traditional implementation in GCMs involve the assumptions GCMs have to make about sub-grid scale cloudiness. While the implementation of a simulator in a GCM outputs one histogram per grid cell, where the simulator itself divides the grid into multiple columns to account for sub-grid scale properties, the implementation online in SAM-CRM-COSP outputs one histogram for the entire domain. In this case, each grid cell of the domain is treated as an individual "sub-grid scale" column, which is cloudy for $\tau > 10^{-7}$, and the entire domain is treated as a large grid cell. As such, since this study focuses on the results for RCE_small, so there will only be one histogram per time step where the temporal average over the ~25 days is analyzed.

Acknowledgments We acknowledge sur

We acknowledge support by NSF AGS 1830724 and NSF AGS 2140419. The authors acknowledge computing support from Cheyenne (https://doi. org/10.5065/D6RX99HX), provided by NCAR's Computational and Information Systems Laboratory, sponsored by the National Science Foundation. We thank all co-authors on the RCEMIP overview paper (Wing et al., 2020a) for providing the RCEMIP simulations as well as Drs. Robert Pincus and Mark Zelinka for their assistance and conversations on certain technical aspects of the procedures used and Dr. Brian Rose for the climlab software. We would also like to thank Dr. Brandon Wolding and two anonymous reviewers for their constructive and thorough reviews. CLS wishes to thank her Ph D committee members: Drs Alvssa Atwood, Mark Bourassa, Eric Chicken, and Guosheng Liu for their support and early feedback on this work.

Data Availability Statement

We thank the German Climate Computing Center (DKRZ) for hosting the standardized RCEMIP data (Wing et al., 2020b), which is publicly available at http://hdl.handle.net/21.14101/d4beee8e-6996-453e-bbd1-ff53b6874c0e. Data derived from the RCEMIP data set (Stauffer, 2023) are archived at https://doi.org/10.5281/zenodo.8270906.

References

Aerenson, T., Marchand, R., Chepfer, H., & Medeiros, B. (2022). When will MISR detect rising high clouds? *Journal of Geophysical Research:* Atmospheres, 127(2), e2021JD035865. https://doi.org/10.1029/2021JD035865

Becker, T., & Wing, A. A. (2020). Understanding the extreme spread in climate sensitivity within the Radiative-Convective Equilibrium Model Intercomparison Project. *Journal of Advances in Modeling Earth Systems*, 12(10), e2020MS002165. https://doi.org/10.1029/2020MS002165

STAUFFER AND WING 21 of 24



- 10.1029/2023MS003738
- Bony, S., & Dufresne, J.-L. (2005). Marine boundary layer clouds at the heart of tropical cloud feedback uncertainties in climate models. Geophysical Research Letters, 32(20), L20806. https://doi.org/10.1029/2005GL023851
- Bony, S., Semie, A., Kramer, R. J., Soden, B. J., Tompkins, A. M., & Emanuel, K. A. (2020). Observed modulation of the tropical radiation budget by deep convective organization and lower-tropospheric stability. *AGU Advances*, 1(3), e2019AV000155. https://doi.org/10.1029/2019AV000155
- Bony, S., Stevens, B., Coppin, D., Becker, T., Reed, K. A., Voigt, A., & Medeiros, B. (2016). Thermodynamic control of anvil cloud amount. Proceedings of the National Academy of Sciences, 113(32), 8927–8932. https://doi.org/10.1073/pnas.1601472113
- Bony, S., Stevens, B., Frierson, D. M. W., Jakob, C., Kageyama, M., Pincus, R., et al. (2015). Clouds, circulation and climate sensitivity. *Nature Geoscience*, 8(4), 261–268. https://doi.org/10.1038/ngeo2398
- Bretherton, C. S., & Blossey, P. N. (2014). Low cloud reduction in a greenhouse-warmed climate: Results from Lagrangian LES of a subtropical marine cloudiness transition. *Journal of Advances in Modeling Earth Systems*, 6(1), 91–114. https://doi.org/10.1002/2013MS000250
- Cess, R. D., & Potter, G. L. (1988). A methodology for understanding and intercomparing atmospheric climate feedback processes in general circulation models. *Journal of Geophysical Research*, 93(D7), 8305–8314. https://doi.org/10.1029/jd093id07p08305
- Chen, Y.-W., Seiki, T., Kodama, C., Satoh, M., Noda, A. T., & Yamada, Y. (2016). High cloud responses to global warming simulated by two different cloud microphysics schemes implemented in the Nonhydrostatic Icosahedral Atmospheric Model (NICAM). *Journal of Climate*, 29(16), 5949–5964. https://doi.org/10.1175/JCLI-D-15-0668.1
- Cronin, T. W., & Wing, A. A. (2017). Clouds, circulation, and climate sensitivity in a radiative-convective equilibrium channel model. *Journal of Advances in Modeling Earth Systems*, 9(8), 2883–2905. https://doi.org/10.1002/2017MS001111
- Dessler, A. E. (2013). Observations of climate feedbacks over 2000-10 and comparisons to climate models. *Journal of Climate*, 26(1), 333–342. https://doi.org/10.1175/JCLI-D-11-00640.1
- Dufresne, J.-L., & Bony, S. (2008). An assessment of the primary sources of spread of global warming estimates from coupled atmosphere-ocean models. *Journal of Climate*, 21(19), 5135–5144. https://doi.org/10.1175/2008JCL12239.1
- Eyring, V., Bony, S., Meehl, G. A., Senior, C. A., Stevens, B., Stouffer, R. J., & Taylor, K. E. (2016). Overview of the Coupled Model Inter-comparison Project Phase 6 (CMIP6) experimental design and organization. Geoscientific Model Development, 9(5), 1937–1958. https://doi.org/10.5194/gmd-9-1937-2016
- Fu, Q. (1996). An accurate parameterization of the solar radiative properties of cirrus clouds for climate models. *Journal of Climate*, 9, 2058–2082. https://doi.org/10.1175/1520-0442(1996)009<2058:AAPOTS>2.0.CO;2
- Hahn, C. J., Rossow, W. B., & Warren, S. G. (2001). ISCCP cloud properties associated with standard cloud types identified in individual surface observations. *Journal of Climate*, 14(1), 11–28. https://doi.org/10.1175/1520-0442(2001)014(0011:ICPAWS)2.0.CO;2
- Hartmann, D. L., & Larson, K. (2002). An important constraint on tropical cloud-climate feedback. Geophysical Research Letters, 29(20), 121–124, https://doi.org/10.1029/2002GL015835
- Held, I. M. (2005). The gap between simulation and understanding in climate modeling. *Bulletin of the American Meteorological Society*, 86(11), 1609–1614. https://doi.org/10.1175/bams-86-11-1609
- Holloway, C. E., Wing, A. A., Bony, S., Muller, C., Masunaga, H., L'Ecuyer, T. S., et al. (2017). Observing convective aggregation. Surveys in Geophysics, 38(6), 1199–1236. https://doi.org/10.1007/s10712-017-9419-1
- Houze, R. A. (2004). Mesoscale convective systems. Reviews of Geophysics, 42(4), RG4003. https://doi.org/10.1029/2004RG000150
- Iacono, M. J., Delamere, J. S., Mlawer, E. J., Shephard, M. W., Clough, S. A., & Collins, W. D. (2008). Radiative forcing by long-lived greenhouse gases: Calculations with the AER radiative transfer models. *Journal of Geophysical Research*, 113, D13013. https://doi.org/10.1029/2008JD009944
- Igel, M. R., Drager, A. J., & van den Heever, S. C. (2014). A CloudSat cloud object partitioning technique and assessment and integration of deep convective anvil sensitivities to sea surface temperature. *Journal of Geophysical Research: Atmospheres*, 119(17), 10515–10535. https://doi. org/10.1002/2014JD021717
- Jakob, C., Singh, M. S., & Jungandreas, L. (2019). Radiative convective equilibrium and organized convection: An observational perspective. Journal of Geophysical Research: Atmospheres, 124(10), 5418–5430. https://doi.org/10.1029/2018JD030092
- Jeevanjee, N., Hassanzadeh, P., Hill, S., & Sheshadri, A. (2017). A perspective on climate model hierarchies. *Journal of Advances in Modeling Earth Systems*, 9(4), 1760–1771. https://doi.org/10.1002/2017MS001038
- Jeevanjee, N., & Zhou, L. (2022). On the resolution-dependence of anvil cloud fraction and precipitation efficiency in radiative-convective equilibrium. *Journal of Advances in Modeling Earth Systems*, 14(3), e2021MS002759. https://doi.org/10.1029/2021MS002759
- Khairoutdinov, M. F., & Randall, D. A. (2003). Cloud resolving modeling of the ARM summer 1997 IOP: Model formulation, results, uncertainties, and sensitivities. *Journal of the Atmospheric Sciences*, 60(4), 607–625. https://doi.org/10.1175/1520-0469(2003)060(0607:CRMOTA)2.0.CO:2
- Kiehl, J. T., Hack, J. J., Bonan, G. B., Boville, B. A., Williamson, D. L., & Rasch, P. J. (1998). The National Center for Atmospheric Research Community Climate Model: CCM3. Journal of Climate, 11(6), 1131–1149. https://doi.org/10.1175/1520-0442(1998)011\langle1131:TNCFAR\rangle2.0.CO;2
- Klein, S. A., & Jakob, C. (1999). Validation and sensitivities of frontal clouds simulated by the ECMWF model. *Monthly Weather Review*, 127(10), 2514–2531. https://doi.org/10.1175/1520-0493(1999)127\(2514:VASOFC\)2.0.CO;2
- Kuang, Z., & Hartmann, D. L. (2007). Testing the fixed anvil temperature hypothesis in a cloud-resolving model. *Journal of Climate*, 20(10), 2051–2057. https://doi.org/10.1175/JCLI4124.1
- Li, J.-L. F., Waliser, D. E., Chen, W.-T., Guan, B., Kubar, T., Stephens, G., et al. (2012). An observationally based evaluation of cloud ice water in CMIP3 and CMIP5 GCMs and contemporary reanalyses using contemporary satellite data. *Journal of Geophysical Research*, 117(D16), D16105. https://doi.org/10.1029/2012JD017640
- Maher, P., & Gerber, E. P. (2019). Atmospheric model hierarchies: Connecting theory and models. *Eos*, 100. https://doi.org/10.1029/2019EO133929 McKim, B., Bony, S., & Dufresne, J.-L. (2023). Physical and observational constraints on the anvil cloud area feedback. *ESS Open Archive*. https://doi.org/10.22541/au.167769953.39966398/v2
- Myers, T. A., Scott, R. C., Zelinka, M. D., Klein, S. A., Norris, J. R., & Caldwell, P. M. (2021). Observational constraints on low cloud feedback reduce uncertainty of climate sensitivity. *Nature Climate Change*, 11(6), 501–507. https://doi.org/10.1038/s41558-021-01039-0
- Noda, A. T., Satoh, M., Yamada, Y., Kodama, C., & Seiki, T. (2014). Responses of tropical and subtropical high-cloud statistics to global warming. *Journal of Climate*, 27(20), 7753–7768. https://doi.org/10.1175/JCLI-D-14-00179.1
- Ohno, T., Noda, A. T., & Satoh, M. (2020). Impacts of sub-grid ice cloud physics in a turbulence scheme on high clouds and their response to global warming. *Journal of the Meteorological Society of Japan. Series II*, 98(5), 1069–1081. https://doi.org/10.2151/jmsj.2020-054
- Ohno, T., Noda, A. T., Seiki, T., & Satoh, M. (2021). Importance of pressure changes in high cloud area feedback due to global warming. Geophysical Research Letters, 48(18), e2021GL093646. https://doi.org/10.1029/2021GL093646

STAUFFER AND WING 22 of 24



- 10.1029/2023MS003738
- Ohno, T., & Satoh, M. (2018). Roles of cloud microphysics on cloud responses to sea surface temperatures in radiative-convective equilibrium experiments using a high-resolution global nonhydrostatic model. *Journal of Advances in Modeling Earth Systems*, 10(8), 1970–1989. https://doi.org/10.1029/2018MS001386
- Ohno, T., Satoh, M., & Noda, A. (2019). Fine vertical resolution radiative-convective equilibrium experiments: Roles of turbulent mixing on the high-cloud response to sea surface temperatures. *Journal of Advances in Modeling Earth Systems*, 11(6), 1637–1654. https://doi.org/10.1029/2019MS001704
- Qu, X., Hall, A. D., Klein, S. A., & Caldwell, P. M. (2014). On the spread of changes in marine low cloud cover in climate model simulations of the 21st century. Climate Dynamics, 42(9–10), 2603–2626. https://doi.org/10.1007/s00382-013-1945-z
- Romps, D. M. (2014). An analytical model for tropical relative humidity. *Journal of Climate*, 27(19), 7432–7449. https://doi.org/10.1175/ JCLI-D-14-00255.1
- Rose, B. E. J. (2018). CLIMLAB: A Python toolkit for interactive, process-oriented climate modeling. *Journal of Open Source Software*, 3(24), 659. https://doi.org/10.21105/joss.00659
- Rossow, W. B., & Schiffer, R. A. (1991). ISCCP cloud data products. Bulletin of the American Meteorological Society, 72(1), 2–20. https://doi.org/10.1175/1520-0477(1991)072<0002:ICDP>2.0.CO:2
- Schneider, S. H., & Dickinson, R. E. (1974). Climate modeling. Reviews of Geophysics, 12(3), 447–493. https://doi.org/10.1029/RG012i003p00447
 Schwarzkopf, M. D., & Ramaswamy, V. (1999). Radiative effects of CH₄, N₂O, halocarbons and the foreign-broadened H₂O continuum: A GCM experiment. Journal of Geophysical Research, 104(D8), 9467–9488. https://doi.org/10.1029/1999JD900003
- Seeley, J. T., Jeevanjee, N., Langhans, W., & Romps, D. M. (2019). Formation of tropical anvil clouds by slow evaporation. *Geophysical Research Letters*, 46(1), 492–501. https://doi.org/10.1029/2018GL080747
- Seeley, J. T., Jeevanjee, N., & Romps, D. M. (2019). FAT or FiTT: Are anvil clouds or the tropopause temperature invariant? *Geophysical Research Letters*, 46(3), 1842–1850. https://doi.org/10.1029/2018GL080096
- Sherwood, S. C., Bony, S., & Dufresne, J.-L. (2014). Spread in model climate sensitivity traced to atmospheric convective mixing. *Nature*, 505(7481), 37–42. https://doi.org/10.1038/nature12829
- Sherwood, S. C., Webb, M. J., Annan, J. D., Armour, K. C., Forster, P. M., Hargreaves, J. C., et al. (2020). An assessment of Earth's climate sensitivity using multiple lines of evidence. *Reviews of Geophysics*, 58(4), e2019RG000678. https://doi.org/10.1029/2019RG000678
- Slingo, A. (1989). A GCM parameterization for the shortwave radiative properties of water clouds. *Journal of the Atmospheric Sciences*, 46(10), 1419–1427. https://doi.org/10.1175/1520-0469(1989)046(1419:AGPFTS)2.0.CO;2
- Soden, B. J., Broccoli, A. J., & Hemler, R. S. (2004). On the use of cloud forcing to estimate cloud feedback. *Journal of Climate*, 17(19), 3661–3665. https://doi.org/10.1175/1520-0442(2004)017h3661:OTUOCFi2.0.CO;2
- Soden, B. J., & Held, I. M. (2006). An assessment of climate feedbacks in coupled ocean-atmosphere models. *Journal of Climate*, 19(14), 3354–3360. https://doi.org/10.1175/JCLI3799.1
- Soden, B. J., & Vecchi, G. A. (2011). The vertical distribution of cloud feedback in coupled ocean-atmosphere models. Geophysical Research Letters, 38(12), L12704. https://doi.org/10.1029/2011GL047632
- Stauffer, C. L. (2023). Cloud feedbacks in radiative-convective equilibrium [Dataset]. Zenodo. https://doi.org/10.5281/zenodo.8270906
- Stauffer, C. L., & Wing, A. A. (2022). Properties, changes, and controls of deep-convecting clouds in radiative-convective equilibrium. *Journal of Advances in Modeling Earth Systems*, 14(6), e2021MS002917. https://doi.org/10.1029/2021MS002917
- Tompkins, A. M., & Craig, G. C. (1998). Radiative-convective equilibrium in a three-dimensional cloud-ensemble model. Quarterly Journal of the Royal Meteorological Society, 124(550), 2073–2097. https://doi.org/10.1002/qj.49712455013
- Tsushima, Y., Iga, S.-I., Tomita, H., Satoh, M., Noda, A. T., & Webb, M. J. (2014). High cloud increase in a perturbed SST experiment with a global nonhydrostatic model including explicit convective processes. *Journal of Advances in Modeling Earth Systems*, 6(3), 571–585. https://doi.org/10.1002/2013MS000301
- Vial, J., Dufresne, J.-L., & Bony, S. (2013). On the interpretation of inter-model spread in CMIP5 climate sensitivity estimates. Climate Dynamics, 41, 3339–3362. https://doi.org/10.1007/s00382-013-1725-9
- Waliser, D. E., Li, J.-L. F., Woods, C. P., Austin, R. T., Bacmeister, J., Chern, J., et al. (2009). Cloud ice: A climate model challenge with signs and expectations of progress. *Journal of Geophysical Research*, 114(D8), D00A21. https://doi.org/10.1029/2008JD010015
- Webb, M. J., Andrews, T., Bodas-Salcedo, A., Bony, S., Bretherton, C. S., Chadwick, R., et al. (2017). The Cloud Feedback Model Intercomparison Project (CFMIP) contribution to CMIP6. Geoscientific Model Development, 10(1), 359–384. https://doi.org/10.5194/gmd-10-359-2017
- Webb, M. J., Senior, C., Bony, S., & Morcrette, J.-J. (2001). Combining ERBE and ISCCP data to assess clouds in the Hadley Centre, ECMWF and LMD atmospheric climate models. Climate Dynamics, 17(12), 905–922. https://doi.org/10.1007/s003820100157
- Webb, M. J., Senior, C. A., Sexton, D. M. H., Ingram, W. J., Williams, K. D., Ringer, M. A., et al. (2006). On the contribution of local feed-back mechanisms to the range of climate sensitivity in two GCM ensembles. *Climate Dynamics*, 27(1), 17–38. https://doi.org/10.1007/s00382-006-0111-2
- Wetherald, R. T., & Manabe, S. (1988). Cloud feedback processes in a general circulation model. *Journal of the Atmospheric Sciences*, 45(8), 1397–1416. https://doi.org/10.1175/1520-0469(1988)045\(\)1397:CFPIAG\(\)2.0.CO;2
- Wing, A. A., Reed, K. A., Satoh, M., Stevens, B., Bony, S., & Ohno, T. (2018). Radiative-Convective Equilibrium Model Intercomparison Project. Geoscientific Model Development, 11(2), 793–813. https://doi.org/10.5194/gmd-11-793-2018
- Wing, A. A., Stauffer, C. L., Becker, T., Reed, K. A., Ahn, M.-S., Arnold, N. P., et al. (2020a). Clouds and convective self-aggregation in a multi-model ensemble of radiative-convective equilibrium simulations. *Journal of Advances in Modeling Earth Systems*, 12(9), e2020MS002138. https://doi.org/10.1029/2020MS002138
- Wing, A. A., Stauffer, C. L., Becker, T., Reed, K. A., Ahn, M.-S., Arnold, N. P., et al. (2020b). Radiative-Convective Equilibrium Model Intercomparison Project (RCEMIP) Simulation Dataset. [Dataset]. WDC Climate. Retrieved from http://hdl.handle.net/21.14101/d4beee8e-6996-453e-bbd1-ff53b6874c0e
- Zelinka, M. D., & Hartmann, D. L. (2010). Why is longwave cloud feedback positive? Journal of Geophysical Research, 115(D16), D16117. https://doi.org/10.1029/2010JD013817
- Zelinka, M. D., & Hartmann, D. L. (2011). The observed sensitivity of high clouds to mean surface temperature anomalies in the tropics. *Journal of Geophysical Research*, 116(D23), D23103. https://doi.org/10.1029/2011JD016459
- Zelinka, M. D., Klein, S. A., & Hartmann, D. L. (2012a). Computing and partitioning cloud feedbacks using cloud property histograms. Part I: Cloud radiative kernels. *Journal of Climate*, 25(11), 3715–3735. https://doi.org/10.1175/JCLI-D-11-00248.1
- Zelinka, M. D., Klein, S. A., & Hartmann, D. L. (2012b). Computing and partitioning cloud feedbacks using cloud property histograms. Part II: Attribution to changes in cloud amount, altitude, and optical depth. *Journal of Climate*, 25(11), 3736–3754. https://doi.org/10.1175/

STAUFFER AND WING 23 of 24



- 10.1029/2023MS003738
- Zelinka, M. D., Klein, S. A., Qin, Y., & Myers, T. A. (2022). Evaluating climate models' cloud feedbacks against expert judgment. *Journal of Geophysical Research: Atmospheres*, 127(2), e2021JD035198. https://doi.org/10.1029/2021JD035198
- Zelinka, M. D., Klein, S. A., Taylor, K. E., Andrews, T., Webb, M. J., Gregory, J. M., & Forster, P. M. (2013). Contributions of different cloud types to feedbacks and rapid adjustments in CMIP5. *Journal of Climate*, 26(14), 5007–5027. https://doi.org/10.1175/JCLI-D-12-00555.1
- Zelinka, M. D., Myers, T. A., McCoy, D. T., Po-Chedley, S., Caldwell, P. M., Ceppi, P., et al. (2020). Causes of higher climate sensitivity in CMIP6 models. *Geophysical Research Letters*, 47(1), e2019GL085782. https://doi.org/10.1029/2019GL085782
- Zelinka, M. D., Zhou, C., & Klein, S. A. (2016). Insights from a refined decomposition of cloud feedbacks. *Geophysical Research Letters*, 43(17), 9259–9269. https://doi.org/10.1002/2016GL069917
- Zhou, C., Dessler, A. E., Zelinka, M. D., Yang, P., & Wang, T. (2014). Cirrus feedback on interannual climate fluctuations. *Geophysical Research Letters*, 41(24), 9166–9173. https://doi.org/10.1002/2014GL062095

STAUFFER AND WING 24 of 24